Development of an Immersion Maskless Lithography System

by

David Chao

B.S. Electrical Engineering, Cornell University (2003)

Submitted to the Department of
Electrical Engineering and Computer Science
in partial fulfillment of the requirements for the degree of

Master of Science

at the

MASSACHUSETTS INSTITUTE OF TECHNOLOGY

September 2005

Author .....
Department of Electrical Engineering and Computer Science
September 6, 2005

Certified by .....
Henry I. Smith
Keithley Professor of Electrical Engineering
Thesis Supervisor

Accepted by .....
Arthur C. Smith
Chairman, Department Committee of Graduate Students

Development of an Immersion Maskless Lithography System

by

David Chao

Submitted to the Department of Electrical Engineering and Computer Science on September 6, 2005, in partial fulfillment of the requirements for the degree of Master of Science

Abstract

As lithography quickly approaches its limits with current technologies, a host of new ideas is being proposed in hopes of pushing lithography to new levels of performance. The work presented in this thesis explores the use of an immersion scheme to improve the performance of a maskless lithographic technique known as Zone-Plate-Array Lithography (ZPAL). This is believed to be the first implementation of an immersion scheme in a maskless lithography system.

This thesis provides a complete description of the Immersion Zone-Plate-Array Lithography (iZPAL) system. Since the zone plate component of the system is largely responsible for its lithographic performance, a thorough analysis of zone plate theory, design, and fabrication is also presented. The focusing performance of an immersion zone plate is then characterized through the experimental reconstruction of its point-spread function. Finally, lithography results obtained with the iZPAL system are compared to those obtained with the non-immersion ZPAL system, demonstrating the improvement in resolution, exposure latitude, and depth-of-focus achieved with the immersion scheme.

Thesis Supervisor: Henry I. Smith
Title: Keithley Professor of Electrical Engineering

Acknowledgements

Seasons come and go, experiments succeed and fail, theories stand and fall apart, but the one thing that has remained constant throughout my two years at MIT has been the group of people I have learned to rely on – the very people responsible for my success.

At the core of this group is Professor Henry Smith. His contagious passion and optimism made even the most daunting of goals appear attainable and worth striving for. He set goals, but gave me tremendous freedom to design my own course of research to meet these goals. This has not only made me a better scientist, it has made me a stronger and more responsible person. The considerable number of distinguished scholars who have once worked and learned under his direction is a testament to him as an advisor. Thank you for giving me the opportunity to be a part of this wonderful team that is the NSL.

Throughout my involvement with ZPAL, I have always thought of Rajesh Menon as a shining example of what it means to be a good researcher. He, more than anyone, has shown me that hard work and dedication are the keys to success. Thank you for being a great role model and for exceeding my expectations as a mentor.

Speaking of exceeding expectations, I've learned that a good officemate does more than just keep his half of the space tidy. Every time I ran into an obstacle, I could always count on Amil Patel, Officemate Version 1.0 and fellow ZPAL teammate, to help as best he could. He would always take my questions seriously, even the 'dumb' ones. And he was always up for a debate, especially when it came to football. Thank you for being a great colleague and friend.

When it came to fabrication, no one was more helpful than Tymon Barwicz. I would probably still be stuck in the early phases of this project if it were not for many of his wonderful insights. Thank you for sharing your knowledge with me. I would also like to thank Feng Zhang for the countless number of times he helped me troubleshoot the Raith150, even during weird hours of the night.

The lab can be a very frustrating place most days. Fortunately, Jim Daley is always around to cheer everyone up. It is remarkable how he manages to keep the lab running so smoothly in addition to assisting anyone (and everyone) in need of help.

Thank you for being so generous with your valuable time. Thanks also to Minghao Qi for keeping me company (and sane) during those many late nights that became early mornings.

I would also like to acknowledge the U.S. Department of Defense for supporting me this past year through the National Defense Science and Engineering Graduate Fellowship.

Success takes the right amount of determination, support, and even a little luck. Thank you fellow NSLers for contributing to my success in so many ways. Thank you also to the rest of my friends for helping me not lose sight of life outside the lab. Thank you to the Wong family for always being enthusiastic about my work and for showing a genuine concern for my well-being. Thank you to my parents and sister for your constant support and encouragement. Even when I questioned my own decisions, you were always there to give me reassurance.

And finally, these acknowledgements would not be complete without thanking my best friend and partner in life, Karen. Thank you for putting up with me and all of my annoying tendencies. Thank you for taking care of everything when I was consumed with work, and even when I wasn't. Thank you for loving me.

Contents

List of Figures

Chapter 1

Introduction – Immersion Maskless Lithography

Much of the groundbreaking research being conducted today in the fields of telecommunications, computer computation, and biology (just to name a few) can largely attribute their successes to the science known as 'Nanotechnology.' Nanotechnology has enabled much of the life we know today, being responsible for many of life's luxuries as well as necessities – from computers for entertainment, to cellphones for communication, to cutting-edge biotechnology for medical breakthroughs. Can one now imagine life without nanotechnology?

At the foundation of all that is nanotechnology lies lithography, its vehicle for existence (its key enabling agent). Lithography, which literally means 'writing in stone,' is a method of printing. One of its earliest manifestations came in the form of engraving patterns onto stone slabs using oil-tipped utensils. The stone slabs were subsequently wet with water-based ink, and since oil repels water, a thin film of ink was left behind wherever the oil was not present. The stones slabs were now ready to be used as stamps for printing. Today, lithography is performed in a number of ways, the most common of which are based on optical, electron, and imprint techniques. Using optical lithography as an example, light is focused onto a photosensitive material, changing its chemical

properties. The pattern is subsequently defined in the material through the use of a developing agent, which selectively removes the areas exposed to the focused optical beam. Since light can be focused down to sub-wavelength dimensions, patterns in the nanometer scale can be created using optical lithography.

1.1 Mask-Based Lithography vs. Maskless Lithography

All forms of lithography can be grouped into two categories: mask-based lithography and maskless lithography. In the mask-based case, an image of a mask containing pre-defined patterns (usually produced using a maskless lithographic approach) is projected

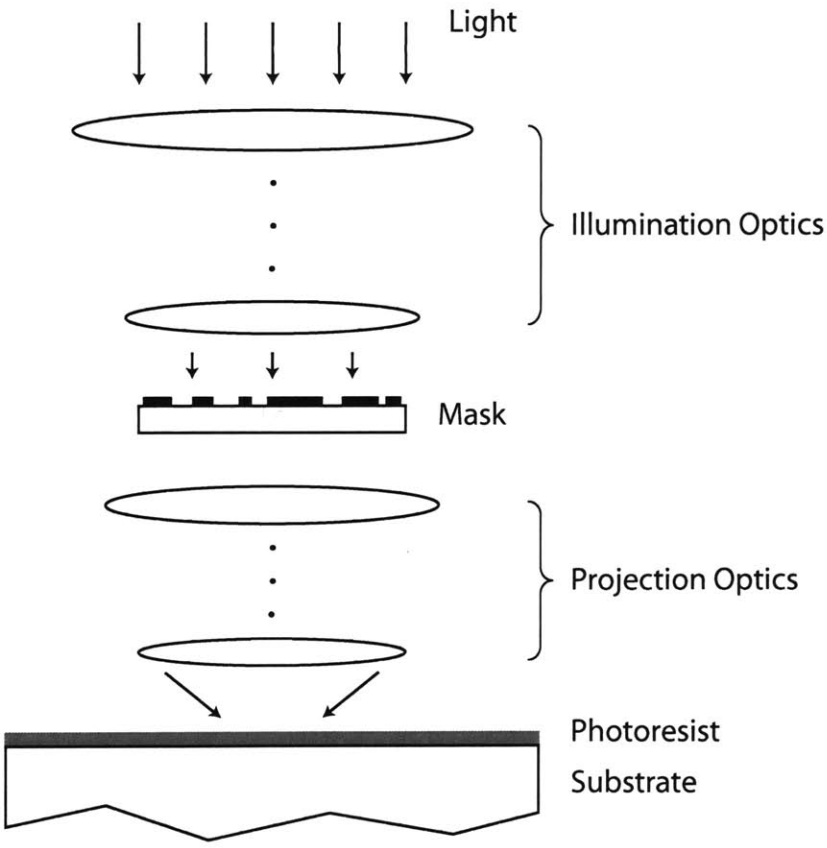

Figure 1-1: Schematic of an optical projection lithography system. The mask-based system images the predefined mask pattern onto the substrate of a photoresist-coated substrate, thereby reproducing copies of the pattern in the photoresist. Note that the details of both the illumination and projection optical systems are not depicted for simplicity, as these systems are typically comprised of tens of lenses.

onto a substrate coated with a thin photosensitive film (photoresist). In this manner, the mask pattern is replicated onto the photoresist, similar to the stone slab example mentioned above. An example of such a system is the optical projection stepper, which is depicted in *Figure 1-1*.

Maskless lithography systems, on the other hand, do not use masks to define patterns onto the photoresist. Instead, lenses are used to focus incident radiation down to a spot on the photoresist, and it is the addition of these discrete spots which eventually forms the desired pattern. *Figure 1-2* illustrates this printing technique, where for instance, a line can be defined through the accumulation of collinear discrete spots. An example of such a system is the electron-beam lithography system depicted in *Figure 1-3*. An electron beam is focused onto the resist coated substrate by means of electric and magnetic fields (the resist in this case is sensitive to electron radiation). A beam blanker is used to turn the electron beam on and off as the substrate is scanned underneath. In this manner, arbitrary patterns can be defined by the addition of discrete spot exposures.

Much of the research to date has been driven by the semiconductor industry, and has centered on the improvement of masked-based lithography systems and its components, from the development of better radiation sources and projection optics, to the enhancement of optical proximity corrections for mask layouts, to the advancement of photoresist chemistries. The reason behind their support for mask-based lithography, such as optical projection lithography, is due to its tremendous throughput advantage

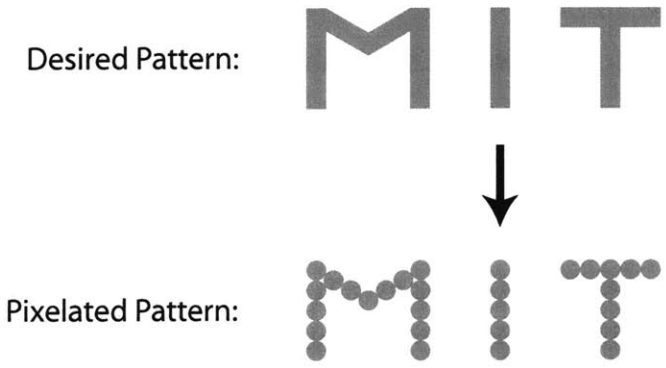

Figure 1-2: Depiction of a maskless lithographic printing technique. Patterns, such as the 'MIT' logo, are broken up into discrete pixels. The sequential exposure of these pixels forms the entire pattern. Any arbitrary pattern can be produced in this manner.

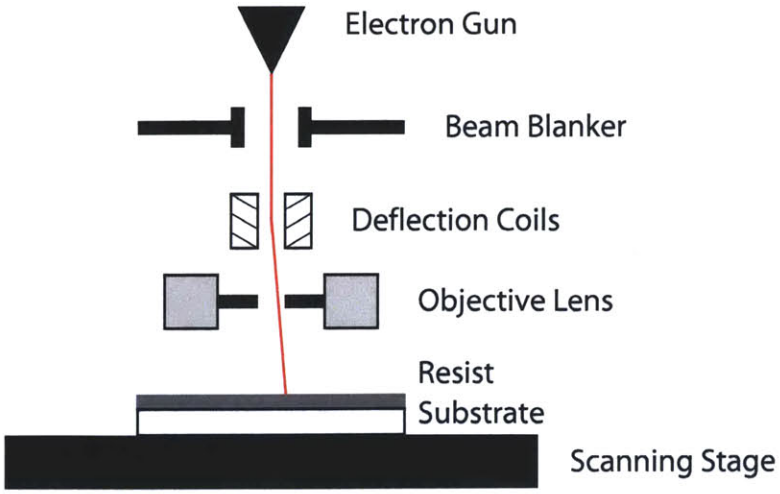

Figure 1-3: Schematic of an electron beam lithography system. Note that this is only a partial depiction of such a system, as many components are left out for simplicity. Electrons emitted by the filament gun are focused by a set of objective lenses to a spot on the substrate. The exact location of this spot on the substrate is controlled by deflection coils. Areas out of its deflection range are brought into range using a scanning stage. A beam blanker effectively turns the electron beam on and off allowing for pixels, and thus patterns, to be exposed in an arbitrary manner.

over maskless lithography. Once a particular chip pattern is defined in a mask, it only takes a fraction of a second for a mask-based system to replicate the entire pattern. This same pattern may take a maskless system days, or even weeks, to reproduce. For mass production purposes, throughput is without doubt a critical figure of merit, therefore justifying the actions of the semiconductor industry.

The majority of other lithography users, however, do not have a need for mass production of Integrated Circuits (ICs). In their case, obtaining a mask for each unique design is probably not the most economical or efficient means for performing lithography. Masks on average tend to be very expensive[1], and it's only getting worse as the technology becomes more advanced and complex [1]. Couple that with the long turnaround time needed for producing masks, and a case for maskless lithography is born. For the majority of lithography users, maskless lithography will save both time and money since each mask will probably be used less than is needed to make up for its cost.

[1] On average, each mask set costs in excess of a few thousand dollars. In some instances, mask sets may cost as much as a million dollars each.

To drive the case home, picture a graduate student feverously working towards a deadline. She does not know for sure if her design will work, so she comes up with multiple iterations to her original design. What should she do, given that all she has access to are mask-based lithography systems? Does she make a mask for each one of her design iterations, thereby wasting valuable money but saving precious time? Or does she make one mask at a time, making another only if the previous design fails, thereby saving money but wasting time? Moreover, even if she has thoroughly thought it through, and has carried out simulations to back up her design decisions, something can and usually will go wrong... I bet she wishes she had to access to a maskless lithography system.

The advantages for eliminating the need for masks do not stop there. The technology required for mask-based lithography systems to compete with maskless lithography systems in terms of performance (resolution, exposure latitude, depth-of-focus) are much more complex compared to that for maskless systems. This complexity makes mask-based lithography systems, on average, cost two to three times more than maskless lithography systems [2].

The increased complexity of mask-based lithography systems also makes modifications to the systems extremely difficult. For instance, changing the radiation source to a shorter wavelength source requires changing the entire illumination and projection optics. While major changes may also need to be made when modifying components to maskless lithography systems, they are generally much less complex.

1.1.1 Maskless Technologies

In the world of maskless lithography, two competing technologies have emerged from the pack – Scanning Spot Technology (SST) and Variable Mask Technology (VMT). SST was used above to explain maskless lithography. In short, radiation is focused down to a spot on the substrate. By turning the radiation to the substrate on and off while the substrate is scanned on a high precision stage, a set of discrete spots are exposed on the substrate. Any arbitrary pattern can be printed using this technique, since all patterns can be decomposed into collections of discrete spots. VMT, on the other hand, borrows much of its configuration from mask-based lithography systems. Picture an optical

projection stepper, such as the one depicted in *Figure 1-1*. Now remove the 'fixed' mask, and replace it with a 'variable' mask. This is the basis of VMT. A 'variable' mask can be programmed to project arbitrary patterns, like a digital projector. In this way, separate masks no longer need to be prepared for each unique design. Instead, arbitrary patterns are defined on a computer, and the computer programs the 'variable' mask to project the desired patterns. Descriptions of systems demonstrating both technologies follow below.

1.1.1.1 Electron-Beam Lithography (SST)

The electron-beam (e-beam) lithography system is the only notable maskless lithography system in production today. It is heavily used in research environments because its ability to pattern without the requirement for masks allows for rapid design prototyping. In addition, these systems provide much higher patterning resolution compared to optical systems[2]. Currently, MIT is in possession of two e-beam lithography systems – the Raith150 and the VS26.

In e-beam lithography, electrons instead of photons are used to chemically alter resist such that areas of the resist exposed to these electrons can be selectively removed with a developing agent. *Figure 1-3* previously depicted such a scanning e-beam lithography system. Electrons are irradiated from a filament gun and focused onto the substrate using electric and magnetic fields. Magnetic deflection coils are placed around the path of the electron beam to deflect the beam to different regions of the substrate. Typically, the deflection system can cover an area at most a few hundred microns in size. In order to pattern larger areas, the stage, on which the substrate sits, is scanned. The collection of exposed spots forms a desired pattern.

Although e-beam lithography offers ultra-high-resolution patterning without the need for masks, it suffers from a problem of throughput. For example, the minimum dwell time for a 6nm stepsize on the Raith150 is 100ns [4]. This roughly translates to a writing time of 77 hours for a 1 cm^2 area. The same 1 cm^2 area can easily be replicated using just one exposure from an optical projection stepper, taking only fractions of a

[2] Feature sizes on the order of 10nm have been demonstrated with e-beam lithography [3].

second in length. However, for design prototyping, e-beam lithography is still the preferred approach by most lithography users.

1.1.1.2 ASML/Micronic's Maskless Lithography System (VMT)

ASML/Micronic employs the variable mask technique in its Sigma7000 Series maskless lithography tool [5]. *Figure 1-4* depicts this system. A spatial light modulator containing

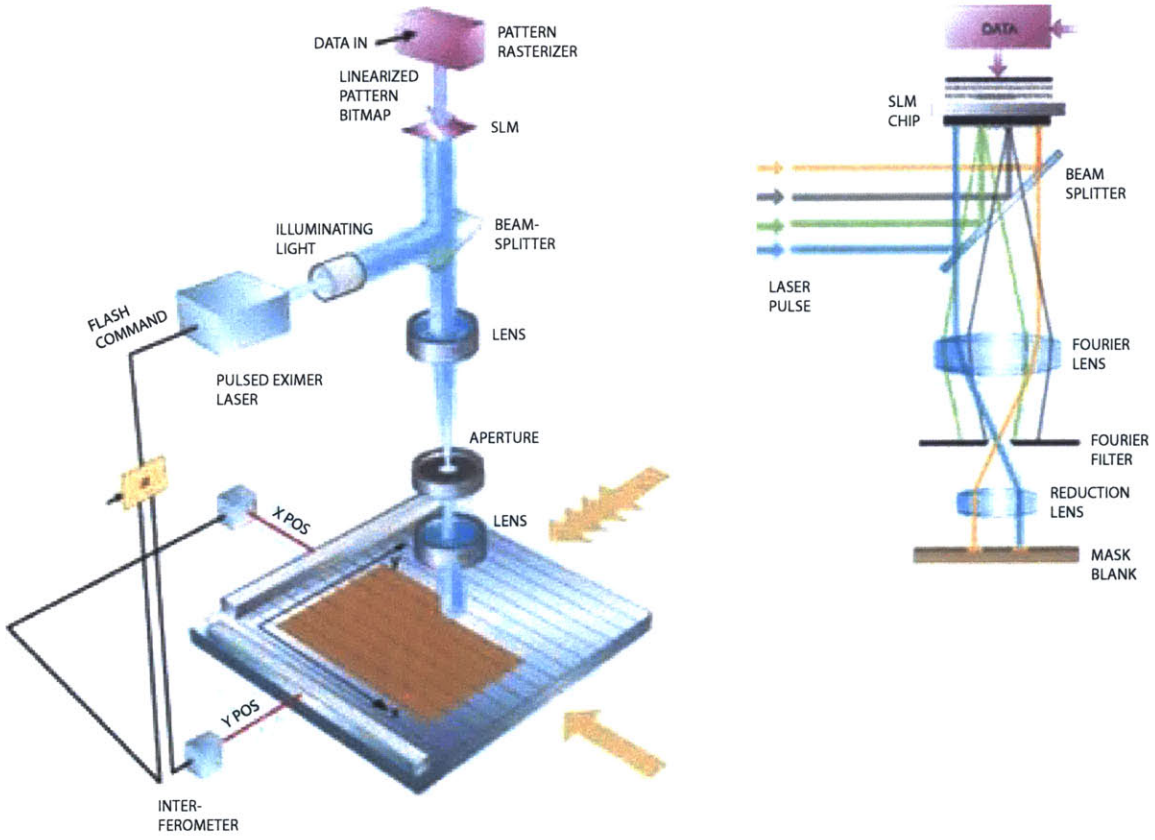

Source: Micronic Laser Systems

Figure 1-4: ASML/Micronic's Sigma7000 Series maskless lithography system. The system replaces traditional masks with a spatial-light modulator (SLM), which in effect acts as a variable mask. The SLM consists of a large array of micromirrors, each capable of reflecting light in one of two directions. An aperture is aligned to pass light reflected in one of these directions while blocking light reflected in the other. In this manner, an arbitrary set of pixels, corresponding to the set of micromirrors reflecting light in the appropriate direction, is exposed on the substrate.

a large array of micromechanical mirrors (~1 million) is used to control the illumination pattern reaching the substrate. Each micromirror in the array is responsible for controlling the illumination to one pixel on the substrate[3]. Illumination to these pixels can individually be turned on and off by electrostatically tilting the micromirrors. An aperture placed between the micromirrors and the substrate serves to only pass light reflected off the untilted micromirrors. In this manner, the computer-controlled spatial light modulator can project any arbitrary pattern onto the substrate.

The rest of the system, i.e. the illumination and projection optics, strongly resembles that of an optical projection stepper. Thus, this system possesses all of the disadvantages listed above for mask-based lithography systems except for those related to the mask. Namely, the system is still extremely complex, and thus inflexible to change.

1.2 Immersion Lithography

Almost everyone has heard of 'Moore's Law,' which states that the number of transistors per square inch on IC chips doubles every year [6]. To keep pace with Moore's Law, lithography tools need to increase their resolution capabilities over this same time period[4]. According to the International Technology Roadmap for Semiconductors (ITRS), lithography tools are expected to pattern 70nm in 2006, 65nm in 2007, 57nm in 2008, 50nm in 2009, and 45nm in 2010[5] [7]. Many tool manufacturers have decided to pursue immersion lithography as a means for meeting these stringent specifications. The benefits of immersion lithography have been known for decades[6], but not until recently has there been a real push for bringing this technology to fruition.

In optical lithography, resolution is generally expressed as:

$$W_{\min} = k_1 \frac{\lambda}{NA}, \tag{1-1}$$

where W_{min} represents the minimum attainable linewidth, k_1 is a proportionality constant which takes into account various system and non-system variables such as system non-

[3] Each micromirror is 16μm x 16μm in size. Reduction optics is placed between the micromirrors and the substrate to scale down the size of the illumination projected from each micromirror.

[4] Resolution must increase by a factor of $\sqrt{2}$ every year to keep pace with Moore's Law.

[5] Currently, lithography tools are patterning at the 80nm node.

[6] The immersion scheme has been practiced in the field of microscopy for over a century.

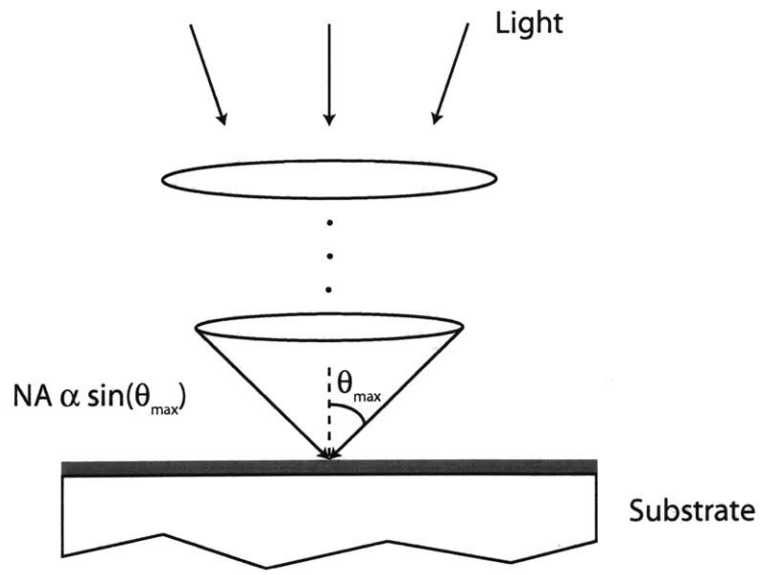

Figure 1-5: A pictorial illustration of the numerical aperture of an optical system.

idealities, resist clipping properties, and environmental conditions, λ is the wavelength of the radiation, and NA is the numerical aperture of the optical system. Reducing W_{min} can be achieved by decreasing k_1, λ or by increasing NA. Since k_1 is a hard to improve, we concentrate on methods for decreasing λ and increasing NA.

We first investigate methods for increasing NA. NA is proportional to $\sin(\theta_{max})$, where θ_{max} is the half-angle of the maximum cone of light focused onto the substrate by the last lens of the projection optics (typically referred to as the convergence half-angle). *Figure 1-5* illustrates this definition schematically. We observe from this figure that an increase in the size of the final lens (in the radial dimension) allows for more light to be focused onto the substrate, resulting in an increase in NA. Unfortunately, there is a limit to this method, as $\sin(\theta_{max})$ has a maximum value of 1. Past some point, increases in the size of the final lens lead to only marginal gains in NA.

Next, we explore possible techniques for reducing λ. The obvious approach would be to use a shorter wavelength radiation source. Most lithography systems need to employ a coherent radiation source, i.e. a laser source. Lasers have been around for 45 years, and in that time period, only a small number of different wavelength laser sources have been invented. Thus, we are limited in the wavelength laser sources we can use {λ = 157nm (F_2), 193nm (ArF), 248nm (KrF), 282nm (XeBr), 308nm (XeCl),

351nm-353nm (XeF), ...}. In addition, problems start to arise in the sub-200nm wavelength regime. The shortened spatial-coherence length of laser sources in this regime becomes a major concern. A further concern is the degradation in transparency of the projection optics at these lower wavelengths. Optical lenses, typically made of glass or fused silica, become opaque at sub-160nm wavelengths.

Another approach for wavelength reduction is immersion of the exposing radiation. The wavelength of the exposing light, λ, can be effectively scaled down to λ/η by introducing a medium (with refractive index η) in-between the final lens and the substrate. For the case of air ($\eta = 1$), λ/η is essentially equal to the wavelength of the radiation source. However, for any other medium ($\eta > 1$) between the final lens and the substrate, the exposing wavelength is effectively reduced and the lithographic resolution concurrently improved (by a factor of η) [8]. With the abundance of high refractive index materials available today and many more in development, this immersion scheme presents a very promising approach to improving lithographic resolution.

Reversal of Conventions

It is important to note that in the analysis above, my convention has been to use the refractive index, η, as a scaling factor for the exposing wavelength. In literature, however, the refractive index is generally coupled into the NA term, i.e. $NA = \eta\sin(\theta_{max})$ [9]. I, nevertheless, find it more logical to introduce the effect of an immersing medium as a reduction of the exposing wavelength, and not as an improvement to NA. However, to be consistent with literature, the remainder of this thesis will take the refractive index into account in the NA equation, and no longer use it as a scaling factor for the exposing wavelength. Hence, the addition of an immersion medium between the final lens and the substrate increases NA (NA can now take on values greater than 1), while λ remains equivalent to the wavelength of the radiation source. In the end, both conventions lead to the same results.

1.2.1 An Immersion Optical Projection Lithography System

One of the many benefits of immersion lithography is its ease of implementation into already existent lithography systems. Take the optical projection stepper as an example. Earlier, it was mentioned that mask-based lithography systems, such as the one currently being considered, are so complex that changes to the system are very costly. Integrating an immersion scheme into such systems is one of the few exceptions to the rule. *Figure 1-6* depicts an immersion optical projection lithography setup. The schematic is identical to the non-immersion optical projection setup shown in *Figure 1-1*, except for the addition of an immersion fluid between the last optical element and the substrate and the modification of a few of the projection optics.

In just under a year, IBM has transformed an optical projection stepper, a 0.75NA

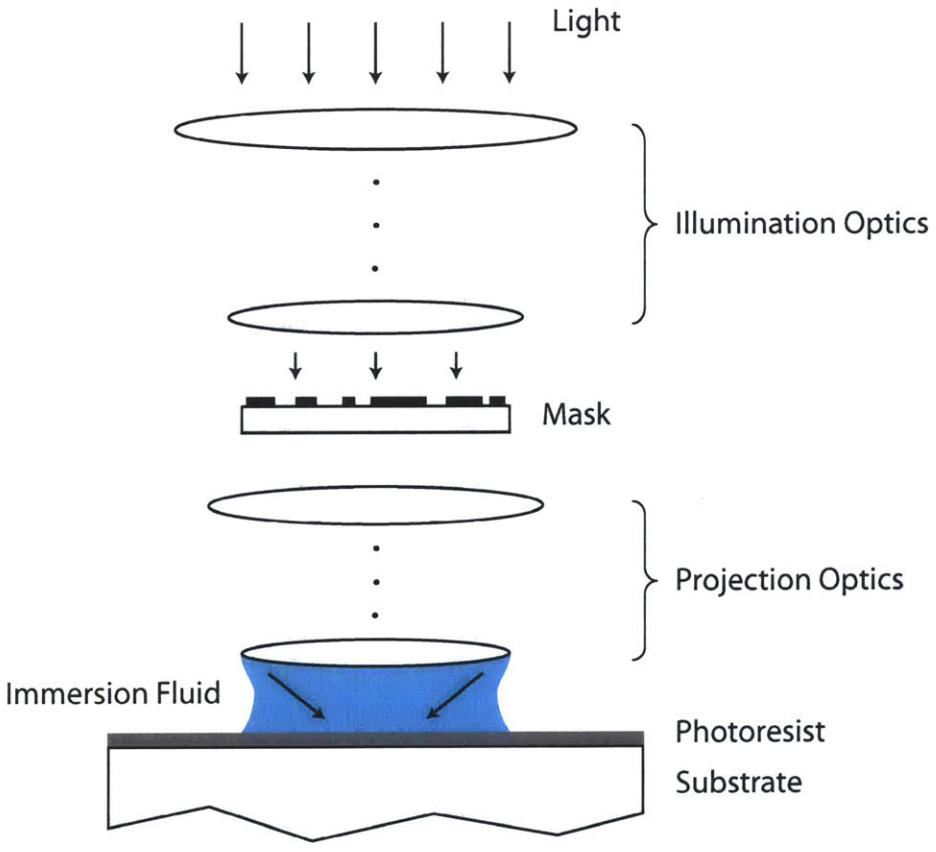

Figure 1-6: Schematic of an immersion optical projection lithography system. Notice that the addition of an immersion fluid between the last optical element and the substrate is the only major difference between this system and the system illustrated in *Figure 1-1*.

ASML AT1150i full-field 193nm projection scanner, into an immersion optical projection stepper [10]. They subsequently used this system to demonstrate the successful patterning of one litho-critical via level of their most advanced 90nm, 64-bit PowerPC microprocessor chip set. The completed microprocessors were fully functional and demonstrated better critical dimension uniformity control compared to those fabricated using the traditional non-immersion process. Furthermore, the exposure did not seem to exhibit many of the problems first thought to be potential showstoppers for immersion lithography. One problem, however, was observed – defects due to microscopic bubbles in the immersion fluid. The effects of these microscopic bubbles were only observed in 17% of the chips, so the yield of the immersion process is still comparable to that of the traditional non-immersion process. What IBM has ultimately done, is to demonstrate the relatively short turnaround time needed for successful implementation of an immersion lithography system. This coupled with the immersion scheme's high resolution capabilities make immersion lithography an ideal technology for moving the field of lithography into the next generation.

1.3 The 1st Immersion Maskless Lithography System

To the best of the author's knowledge, the work presented in this thesis describes the first implementation of an immersion maskless lithography system. Maskless lithography and immersion lithography have been investigated for many years, with a number of systems based on these technologies having been developed and many more currently in development. However, so far none of these systems have incorporated both the maskless and immersion concepts into one system. Immersion Zone-Plate-Array Lithography (iZPAL) is the first system to accomplish such a feat. iZPAL employs SST (Scanning Spot Technology) like an e-beam lithography system. However, unlike an e-beam lithography system which uses a single electron beam to expose spots in a serial manner, iZPAL utilizes a massive parallel array of optical beams, giving it a tremendous throughput advantage over most other SST-based lithography systems. The next chapter describes the iZPAL system in detail.

Chapter 2

Immersion Zone-Plate-Array Lithography: System Description and Experimental Operation

Immersion Zone-Plate-Array Lithography (iZPAL) is an innovative optical maskless technology that employs an immersion scheme to further improve its lithographic performance. As was discussed in Chapter 1, most immersion lithography systems are implemented through the modification of existing non-immersion lithography systems. iZPAL is no different in this respect. ZPAL itself is a maskless lithography system, and its configuration is nearly identical to that of iZPAL. Therefore, we proceed by first providing a system description of ZPAL. We then describe the steps used to transform ZPAL into iZPAL. At the very end, a description of iZPAL's experimental setup procedure is provided.

2.1 Zone-Plate-Array Lithography (ZPAL)

ZPAL is an optical maskless technique that operates on the principle of diffraction rather than refraction. Instead of a single massive lens, an array of thousands of nanofabricated Fresnel zone plate lenses is used, each focusing a beam of light onto the substrate. A

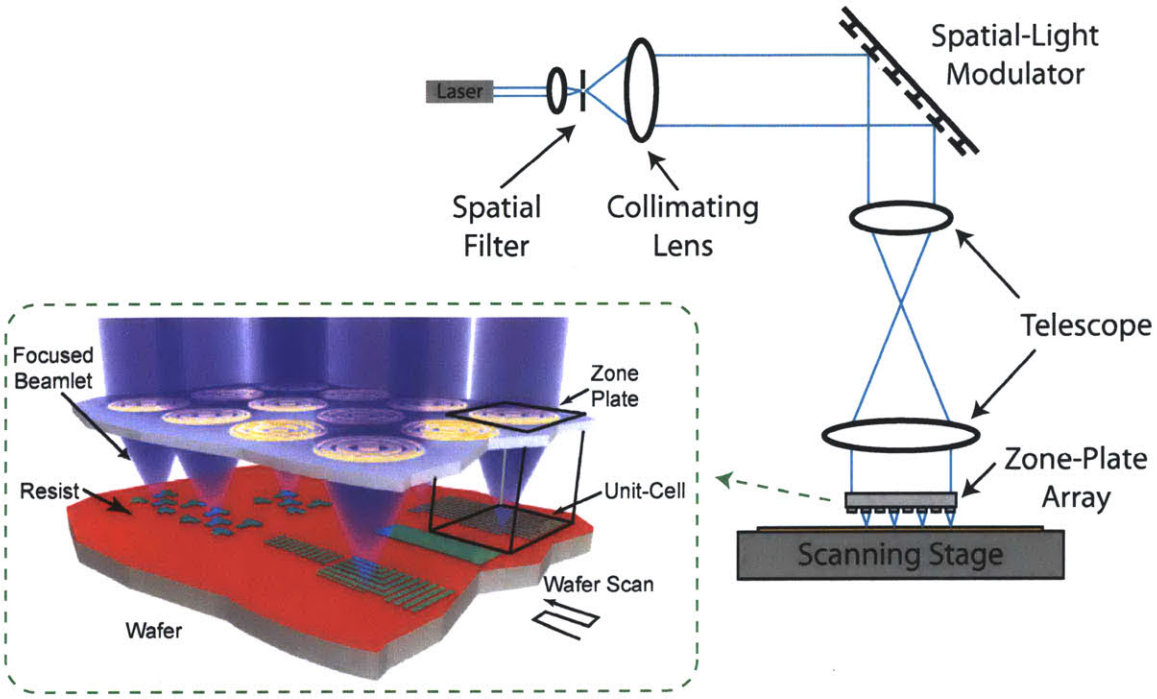

Figure 2-1: Schematic of Zone-Plate-Array Lithography (ZPAL). Light emitted from a laser source passes through a spatial filter, which 'cleans up' the beam, before illuminating the spatial-light modulator (SLM). The SLM controls the intensity of light incident on each zone plate of the zone-plate array. The zone plates focus these incident radiation beamlets onto the substrate as the substrate is scanned. Patterns of arbitrary geometries are thus patterned in a 'dot-matrix' fashion.

computer-controlled array of micromechanical spatial light modulators turns the light to each lens on or off as the substrate is scanned under the array, thereby enabling patterns of arbitrary geometries to be printed in a 'dot-matrix' fashion [11-14]. A schematic of ZPAL is shown in *Figure 2-1*.

The figure above illustrates ZPAL's patterning strategy. Each zone plate is responsible for writing a section of the total pattern[1]. These sections, labeled 'unit-cells' in the figure above, are written in parallel. The full pattern is then formed through the stitching together of these unit-cells. If we assume that the zone-plate array is as large as (or larger) than the pattern to be written, then the time needed to expose the entire pattern is equivalent to the time it would take for one zone plate to write its unit-cell. Hence,

[1] The size of these sections depends on the spacing of the zone plates in the zone-plate array. For densely packed zone plates, the size of these sections is approximately equal to the size of the zone plates.

ZPAL solves the throughput problem faced by most other maskless lithography technologies[2].

2.2 ZPAL's Key Components

Figure 2-2 provides a photograph of our prototype ZPAL system along with a block diagram illustrating ZPAL's operation flow. All of ZPAL's key components are labeled in the figure. They are: the radiation source, the spatial light modulator, the zone-plate array, the scanning stage, and the control computer. Each of these components is described in more detail.

2.2.1 The Radiation Source

Zone plates can focus any wavelength radiation with one stipulation – the radiation must be coherent, both temporally and spatially. This requirement narrows our choice of radiation sources down to the limited number of laser sources available today. Of those, the lower wavelength sources are appealing from a resolution standpoint. However, the lowest wavelength sources (sub-200nm) are impractical for ZPAL due to their low spatial coherence lengths and low power outputs. These reasons ultimately led us to choose a 400nm Gallium-Nitride (GaN) solid-state laser. This laser source gives ZPAL the capability of patterning down to sub-200nm features.

2.2.2 The Spatial Light Modulator

The secret behind ZPAL's maskless parallel patterning strategy was revealed at the beginning of this chapter. There, it was mentioned that all the zone plates in the zone-plate array pattern simultaneously, but do so independently of one another. This is accomplished by controlling the intensity of the light incident on each of these zone plates using a micromechanical spatial light modulator placed appropriately between the radiation source and the zone-plate array. Two such technologies have been explored for

[2] ZPAL's throughput is still orders of magnitude lower than most mask-based lithography technologies, but is orders of magnitude higher than many maskless lithography technologies, such as scanning electron beam lithography for example.

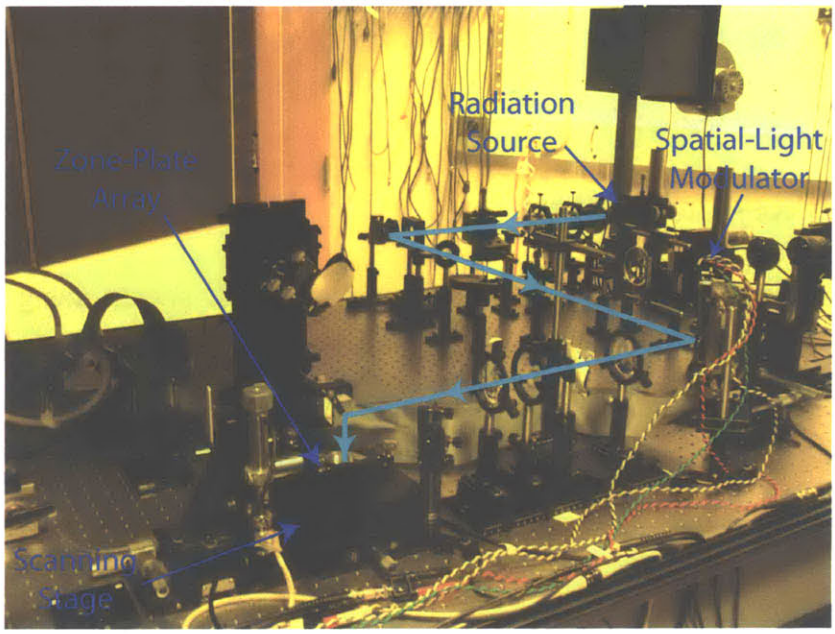

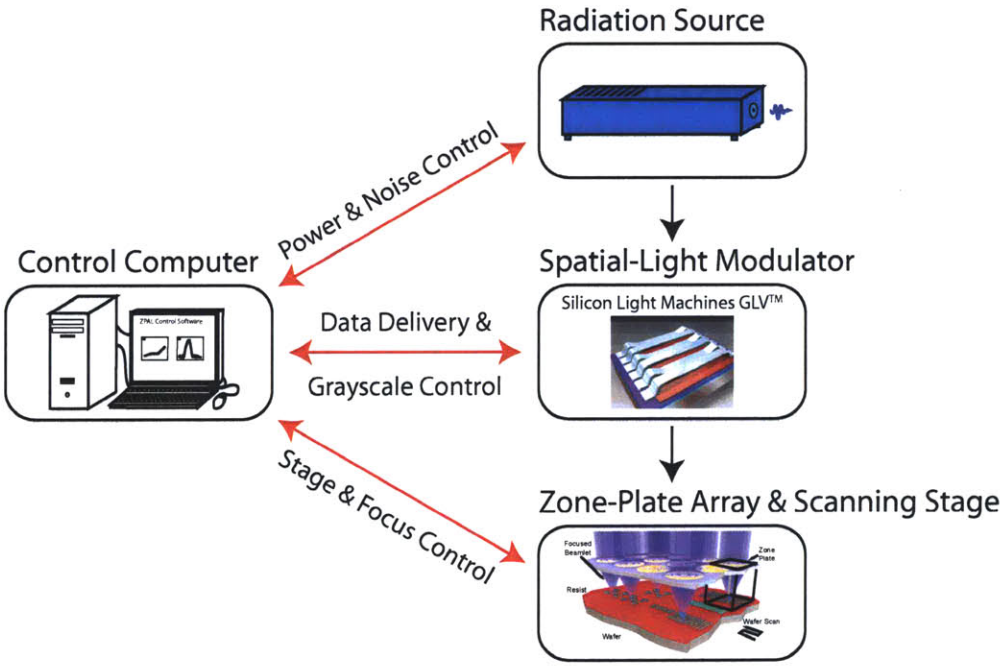

Figure 2-2: Photograph of the prototype ZPAL system. The path of light travel is traced out in 'light blue.' A computer (not pictured) synchronizes the operation of ZPAL's key components, the details of which are outlined in the block diagram.

ZPAL – a Digital Micromirror Device (DMD) manufactured by Texas Instruments and a Grating Light Valve™ (GLV™) manufactured by Silicon Light Machines [15-16].

The DMD contains over a million independently controlled micromirrors. These micromirrors have the ability to arrange themselves in one of two positions. Normally, the micromirrors are in the 'flat' position. When electrostatic forces are applied to particular micromirrors, those micromirrors rotate to a 'tilt' position. Thus, light incident on this device is reflected in one of two possible directions. This technology can be utilized in ZPAL to control the light incident to each zone plate. A schematic of the DMD's implementation in ZPAL is shown in *Figure 2-3*. The micromirror array is aligned such that light reflected off the micromirrors in the 'flat' position are incident normal to the zone-plate array while light reflected off the micromirrors in the 'tilt'

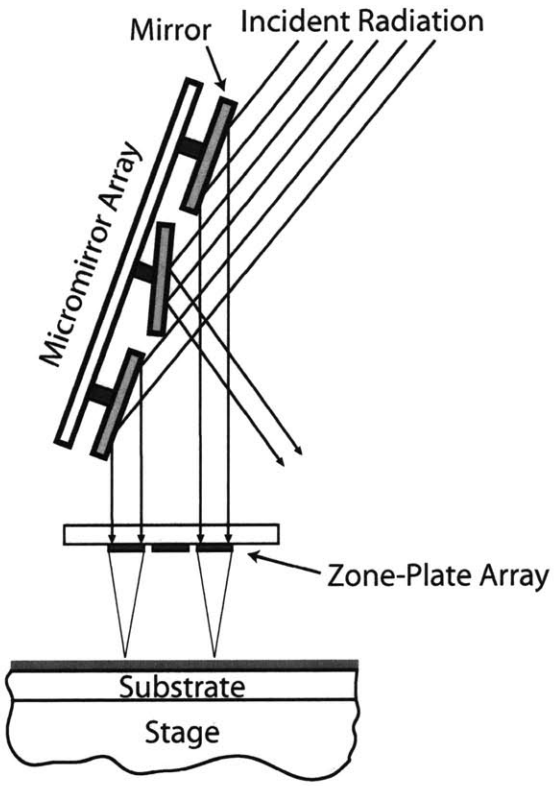

Figure 2-3: Implementation of the Digital Micromirror Device (DMD) in ZPAL. Each micromirror can arrange itself in one of two positions, and can therefore reflect light in one of two directions. The DMD is aligned such that light traveling in one of the two reflected directions is normally incident on the zone-plate array, while light traveling in the other reflected direction misses the zone-plate array.

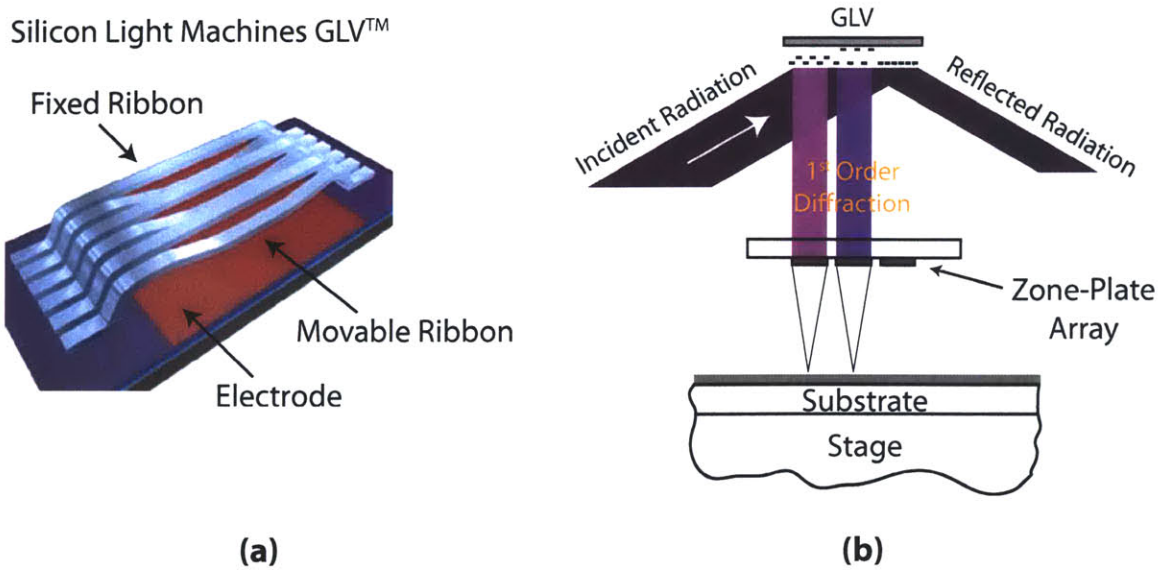

Figure 2-4: Implementation of the Grating Light Valve™ (GLV™) in ZPAL. Each GLV™ pixel depicted in **(a)** can either form a planar surface to reflect light or a grating to diffract light. The GLV™ is aligned such that light diffracted into the +1 order is normally incident on the zone-plate array, as illustrated in **(b)**. Thus, the GLV™ effectively turns light to the zone plates on and off by diffracting or reflecting light respectively. Note that the amount of light diffracted into the +1 order can also be controlled by appropriately adjusting the depth of its grating.

position propagate away from the zone-plate array[3]. Telescoping optics are placed between the micromirrors and the zone-plate array to map one micromirror to one zone plate.

In contrast to the DMD, the GLV is a diffraction-based technology comprised of over a thousand independently controlled elements. Each GLV pixel consists of six Aluminum (Al) ribbons in parallel. When inactivated, the GLV pixel acts like a mirror and reflects light at an angle equal to the angle at which it was incident. When activated, however, electrostatic forces are used to pull down alternating ribbons of the GLV pixel, forming a phase grating. Light incident on this grating will diffract in many different angles, i.e. diffraction orders. Since light diffracted in these diffraction orders can be turned on and off by simply activating or inactivating the GLV pixel, such a technology

[3] The DMD can be also be aligned so that micromirrors in the 'tilt' position reflect light to the zone-plate array and micromirrors in the 'flat' position reflect light away from the zone-plate array.

can be used in ZPAL to control the light incident to each zone plate. A schematic of the GLV's implementation in ZPAL is shown in *Figure 2-4*, along with a depiction of one GLV pixel in operation. The GLV is aligned such that the +1 diffraction order is incident normally on the zone-plate array. All other diffraction orders, including light reflected off a non-actuated GLV pixel, are deflected away from the zone-plate array. As was done with the DMD, telescoping optics are placed between the GLV and the zone-plate array to map one GLV pixel to one zone plate.

The GLV technology has some inherent advantages over the DMD technology for ZPAL. The process used by the GLV for switching light to a zone plate (ribbon pull-down) is intrinsically much faster than that used by the DMD (micromirror tilting). For a quantitative comparison, it takes the DMD 20μs to turn off light to a zone plate, while it only takes the GLV 20ns. That's a three orders of magnitude improvement! The GLV also has built-in grayscaling[4], something the DMD does not. Grayscaling in the GLV is accomplished by controlling the depth at which the ribbons are pulled down. This, in effect, determines the amount of light diffracted into the +1 order. These two advantages make the GLV a better multiplexing element for ZPAL, and is currently being used as such [17].

2.2.3 The Zone-Plate Array

The zone plates are the single most innovative and important part of the ZPAL system, as they are largely responsible for the system's lithographic performance. ZPAL departs from century old refractive technologies in introducing the use of diffractive optics, i.e. zone plates, for lithography. We discuss the differences between these two technologies below. The zone plate, however, deserves its very own chapter, so we hold off on its analysis until the next chapter.

[4] Grayscaling is used to correct for any variations in the efficiencies of the zone plates. It is also important for applications such as proximity effect correction (PEC).

2.2.3.1 Diffractive vs. Refractive Lens Technologies

Zone plates can simply be thought of as optical lenses. They behave very much like traditional optical lenses, but differ in one important respect – they use the principle of diffraction, not refraction, to focus light. Light, being a wave, has two components – an amplitude and a phase component. The phase component is the key to diffraction theory. As a motivating example, imagine two waves with equal amplitudes traveling in parallel. These waves, although equal in amplitude, will cancel each other out if their phases differ by π radians. Now it's clear how diffractive lenses work to focus light – they constructively interfere all transmitted light at its focal point. Light that would normally destructively interfere at this point is either blocked or manipulated to constructively interfere there. It is for this reason that diffractive lenses need coherent illumination.

Refractive lenses, on the other hand, operate under Snell's Law, i.e. incident light is bent in varying degrees so that it all crosses at a common point. *Figure 2-5* illustrates this process. The curvature of refractive lenses is designed such that light further from the optical axis is bent more than light closer to the optical axis, leading to a common crossing point.

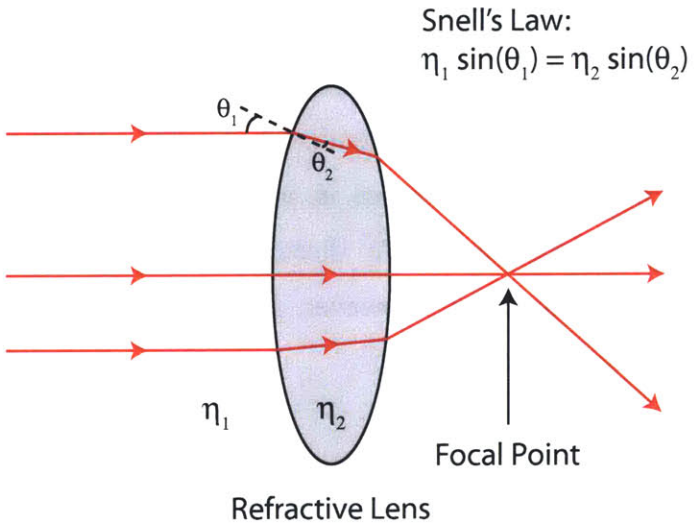

Figure 2-5: The refractive process for focusing light. A refractive lens bends light according to Snell's Law. Its curvature, which determines the degree of light bending, can therefore be designed to direct all incident light to a common point.

Diffractive lenses have numerous advantages over refractive lenses, due in large part to the superior fabrication techniques used for their production. Diffractive lenses are made using nanofabrication processes, where dimensions can be controlled to the nanometer scale. Refractive lenses, on the other hand, continue to rely on ancient techniques such as mechanical polishing. These techniques are not as precise as the ones used to produce their diffractive counterparts. Nanofabrication processes are also much more repeatable. As a result, better uniformity can be achieved across a larger array of diffractive lenses. As a further advantage, nanofabrication processes exhibit nanometer placement accuracy, which is extremely important for stitching together fields exposed in parallel (ala ZPAL). One final advantage diffractive lenses have over refractive lenses is its scalability to lower and lower wavelengths. Refractive lenses, because they are typically made of glass or fused silica, become opaque at sub-160nm wavelengths.

2.2.4 The Scanning Stage

A precision scanning stage is used to raster scan the substrate during an exposure. The stage positioning accuracy plays a major role in determining how close exposed patterns are to ideal. It affects critical dimension control, pattern placement, and stitching. The scanning stage must also have enough range to scan an area the size of a unit-cell. With this in mind, we chose the Piezo Flexure Nanopositioning Scanner from Physik Instrumente (model P-770), which offers a scan range of 200μm x 200μm and a positioning accuracy of less than 10nm. Velocity feedback circuits were then custom built to enable continuous-velocity scanning of the stage. The continuous scan mode vastly improves exposure times (throughput).

2.2.5 The Control Computer

A computer equipped with LabVIEW software and controllers for the spatial light modulator and scanning stage is used to run ZPAL. A custom-written LabVIEW program handles the exposure. First, the pattern to be exposed is encoded in a readable format and loaded into the LabVIEW program. The program then divides the pattern into unit-cells and sends the appropriate data to each pixel of the spatial light modulator. It

simultaneously synchronizes the motion of the scanning stage so that everything works in unison.

2.3 Transforming ZPAL into iZPAL

iZPAL is depicted in *Figure 2-6*. The system depicted in this figure is very similar to the non-immersion ZPAL system depicted in *Figure 2-1*. There are, however, two major differences between the systems. The more obvious of the two differences is the change in the medium between the zone-plate array and the substrate from air (ZPAL) to a high-index immersion fluid such as deionized-water (iZPAL). The other difference, which may not be immediately apparent from looking at the two figures, is the zone plates themselves. The medium in which the zone plate focuses its radiation influences its design. Thus, the zone plates used in ZPAL cannot be used in our immersion experiments.

Replacing the air between the zone-plate array and the substrate with deionized-

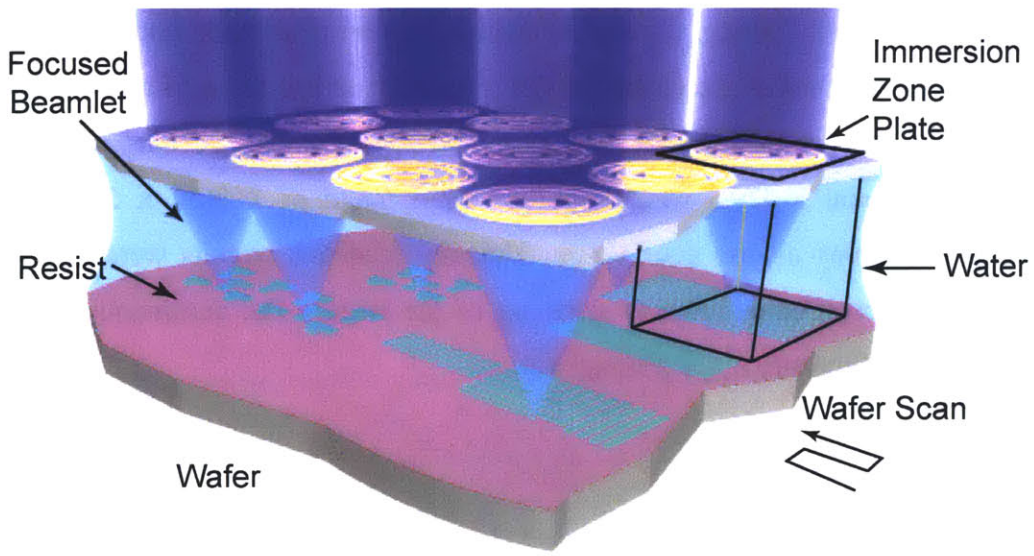

Figure 2-6: Schematic of Immersion Zone-Plate-Array Lithography (iZPAL). The space between the zone-plate array and the substrate is filled with DI-water. An array of specially designed zone plates focuses incident radiation beamlets through the water and onto the surface of the substrate. The rest of this system's operation is identical to that of the non-immersion ZPAL system.

water (DI-water) is not as simple as it may appear. The zone plates are designed to have a focal length of 40μm. Thus, the gap between the zone-plate array and the substrate is too small to push DI-water in through its sides. Instead, a micropipette is used to place a drop of DI-water (volume ≈ 800nL) onto the substrate. The zone-plate array is then aligned to the droplet using a bright-field microscope and lowered until a gap of 40μm is reached. The small gap prevents rapid evaporation of the DI-water into the surrounding air, allowing exposures that are hours in length to be completed with only one droplet of DI-water.

The redesign of the zone plates for this new medium is fairly straightforward. It requires nothing more than changing the value of one parameter in the design. The fabrication of these new zone plates, however, is another story. The process used for the fabrication of non-immersion zone plates cannot be used for the fabrication of immersion zone plates for reasons explained later. Therefore, a new fabrication process with new starting materials was developed. The zone plate design and fabrication process is discussed in further detail in the next chapter.

2.4 Experimental Setup Procedure

A step-by-step procedure for setting up an iZPAL exposure:

- Place a silicon wafer coated with Barli anti-reflection coating (200nm) and PFI-88 photoresist (100nm) on the scanning stage.
- Turn on the vacuum to the scanning stage to prevent the substrate from moving.
- Parallelize the zone-plate array to the substrate.
- Add a droplet of DI-water onto the substrate using a micropipette.
- Align the zone-plate array to the water droplet using a bright-field microscope.
- Lower the zone-plate array onto the water droplet using a z-stage.
- Gap the zone-plate array to the substrate.
- Run the exposure using the custom LabVIEW program.

The parallelization and gapping of the zone-plate array to the substrate are explained in more detail below.

2.4.1 Parallelization

The zone-plate array needs to be parallel with the substrate to ensure that all the zone plates in the array can be properly gapped. The depth-of-focus of our zone plates, i.e. the maximum distance away from a zone plate's focal plane such that its focused light is only marginally degraded, is no more than a few hundred nanometers. The zone-plate array, however, can be millimeters or even centimeters in both length and width. Therefore, even the slightest of tilts[5] will cause non-uniform patterning across the zone plates in the array (that is, if they pattern at all). For example, assume the zone-plate array is 1mm x 1mm in size. A mere tilt of 0.1 degrees corresponds to a 1.75μm difference in gap between zone plates located on opposite ends of the zone-plate array.

A technique that can detect even the slightest of tilts is needed. The Mach-Zender interferometer does this. *Figure 2-7* illustrates a typical Mach-Zender setup, which is nearly identical to the one used for iZPAL. In this interferometer, light reflected off two

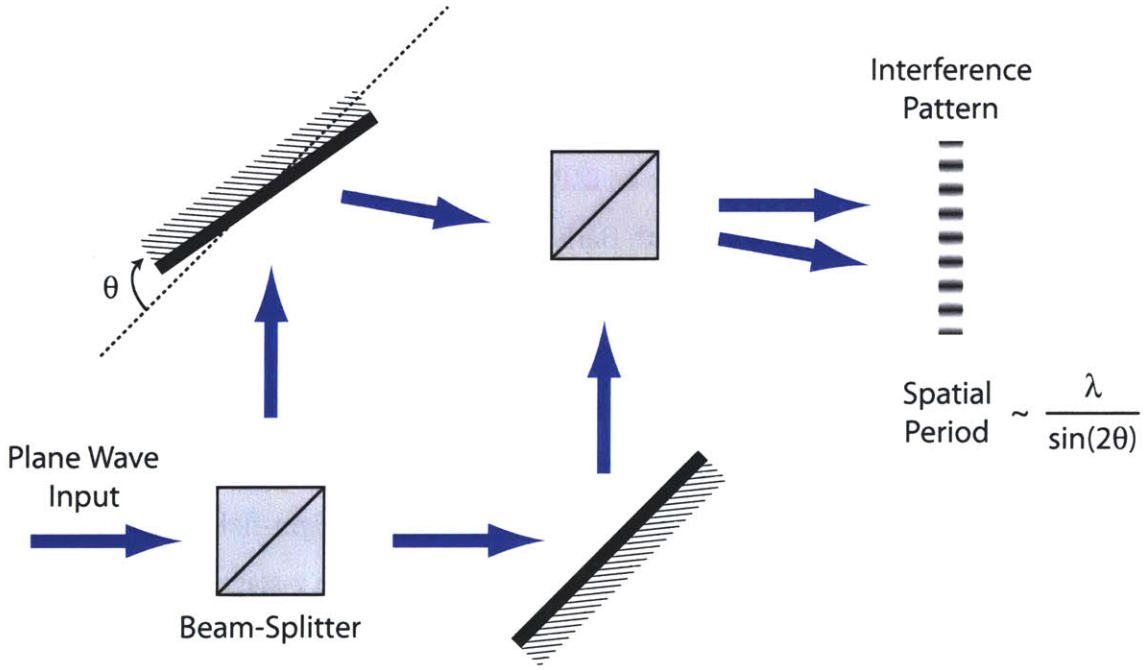

Figure 2-7: A Mach-Zender interferometer setup similar to the one used to parallelize the zone-plate array to the substrate.

[5] 'Tilt' in this context means the relative tilt of the zone-plate array in reference to the substrate.

unparallel surfaces will interfere and display interference fringes at the detector. The period of these fringes, given that one surface is tilted θ degrees in reference to the other, is $\lambda/\sin(2\theta)$. Therefore, we can minimize the tilt, θ, by maximizing the period of the fringes seen at the detector. In my experiments, a maximum fringe period was a few millimeters, which corresponds to a tilt of 0.005 degrees (parameters used: fringe period = 4mm, λ = 632.8nm).

2.4.2 Gapping

As mentioned above, the depth-of-focus of our zone plates is at most a few hundred nanometers. This implies that there's little room for error in the gapping of the zone-plate array to the substrate. If the gap is off in either direction by more than a few hundred nanometers, the zone plates won't pattern properly or won't pattern at all.

It turns out that zone plates can be used for confocal microscopy [18]. *Figure 2-8* illustrates such a setup. We exploit this property of zone plates to accurately gap them to the substrate. Light incident on the zone plates is focused onto the substrate. Some of this light reflects back from the substrate and is reimaged by the zone plates. At precisely the correct gap, the zone plates focus incident light down to a spot on the substrate and recollimate all the light reflected back. A second lens (refractive) and an aperture are positioned such that the light recollimated by the zone plates is focused by this second lens down to a spot at the aperture. The aperture blocks light reimaged by the zone plates at all other gaps. Therefore, a detector placed on the other side of the aperture will detect a signal only when the zone plates are perfectly gapped to the substrate.

There is one additional complication. The gapping procedure described above relies on the projection and reflection of light onto and back from the substrate, exposing the photoresist in the process. Therefore, this procedure can only be performed using a wavelength light to which the photoresist is insensitive[6]. Zone plates designed to focus this new radiation (HeNe) are fabricated together with the zone-plate array and appropriately positioned around its perimeter. Proper gapping of the HeNe zone plates

[6] The photoresist used in our experiments, PFI-88, is insensitive to HeNe light (λ=632.8nm).

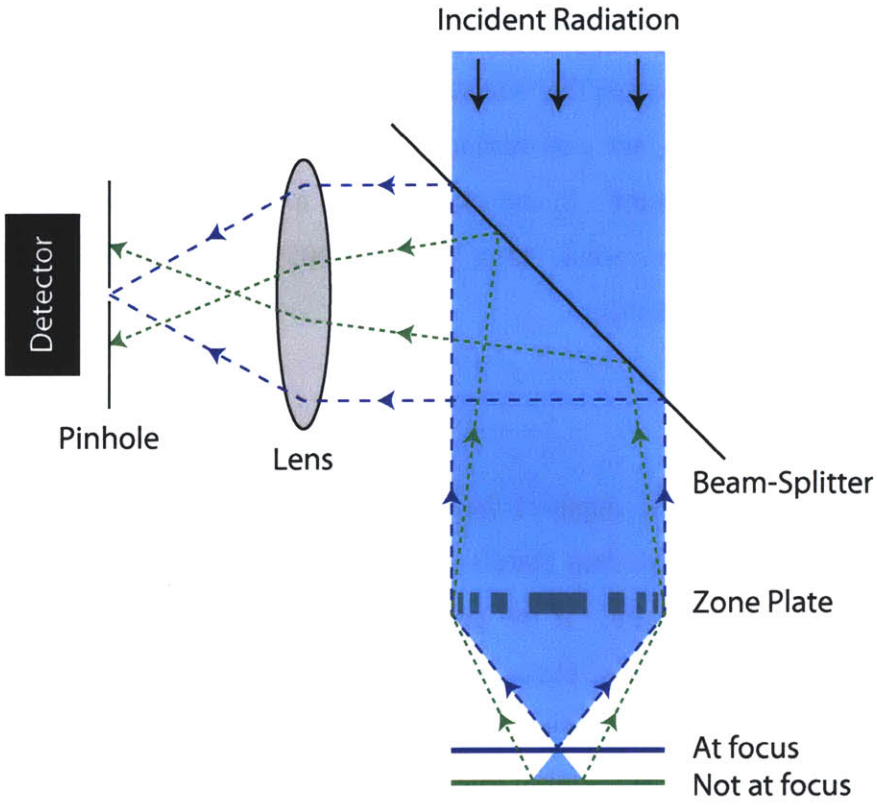

Figure 2-8: The confocal microscopy setup used to gap the zone-plate array to the substrate. The zone plates themselves are used to image light reflected back from the substrate. In the setup, only light re-collimated by the zone plates pass through the pinhole and reach the photodetector. The zone plates only re-collimate the back-reflected light when they are perfectly gapped to the substrate.

ensures the proper gapping of the zone-plate array since both sets are designed to have the same focal length.

Chapter 3

Zone Plates:

Theory, Design, and Fabrication

Although the application of zone plates for lithography has only very recently been proposed and investigated, zone plates themselves have been around for over a century. Zone plates were derived from the work of Fresnel, particularly his concept of Fresnel zones, in the 1800's. To this day, it is unknown who first succeeded in experimentally demonstrating its proper functionality, though there are a few theories as to who it may be. For instance, Lord Rayleigh of 'Rayleigh Scattering' fame wrote in a notebook entry on April 11th, 1871: "The experiment of blocking out the odd Huygens zones so as to increase the light at centre succeeded very well" [19]. Today, however, most people give Fresnel the credit to the discovery of these diffractive optical elements and refer to them as Fresnel zone plates. The rest, as the say, is history.

3.1 Zone Plate Theory

As has been mentioned numerous times in the past, zone plates focus light using the principle of diffraction. Light, being a wave, has two components – an amplitude and a phase component. It is the phase component which is key to diffraction. I've used the following example before to motivate this point: Imagine two waves with equal amplitudes traveling in parallel. These waves, although equal in amplitude, will cancel each other out if their phases differ by π radians. Therefore, one can think of a zone plate as a device which manipulates light in a manner such that all light constructively interferes at its focal point.

Let me clarify the previous statement schematically (see *Figure 3-1*). First, imagine light incident normally (plane wave) on a device which is either circular, rectangular, or any other arbitrary shape. Light passes through this device and continues on its way, but not before it is altered in some manner. The device, it turns out, has manipulated the light such that all the light constructively interferes at **P** (the focal point of the device). The question now is, how does the device achieve this?

For the explanation, we once again examine the phase component of light, since it is this component which determines the light's constructive or destructive behavior. The phase component is expressed as:

$$e^{-i\left(\frac{2\pi}{\lambda/\eta}\right)l}, \tag{3-1}$$

where l represents the distance traveled by the light [20]. *Figure 3-2* plots the real part of this phase component as a function of l. Two important observations are made from this plot. First, the phase component is periodic with period equal to λ/η. Second, the phase component takes on positive values for a span of $\lambda/2\eta$, then negative values for a span of $\lambda/2\eta$, then positive values again for a span of $\lambda/2\eta$, and so on and so forth. These two properties of the phase component help explain the zone plate's operation.

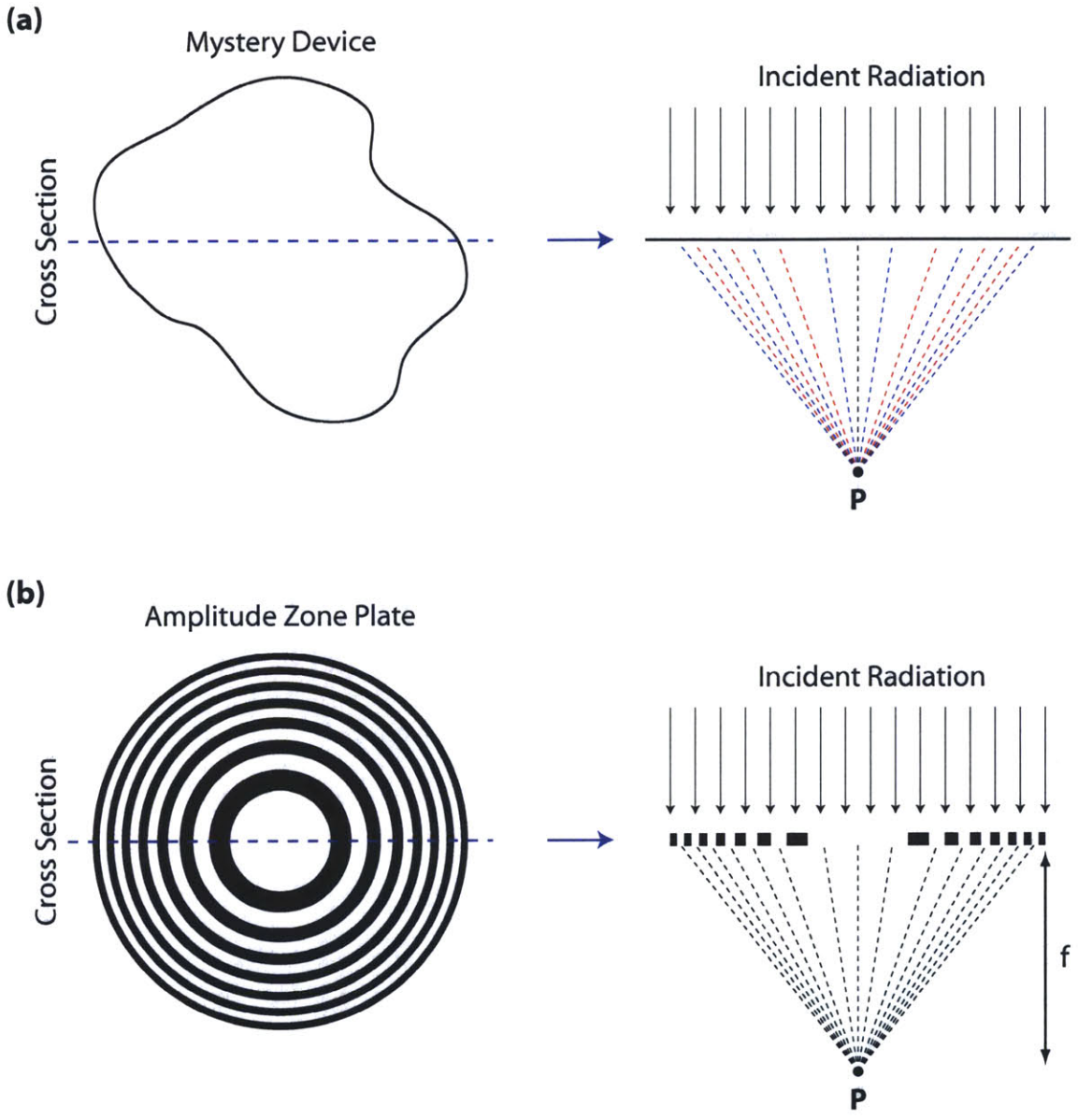

Figure 3-1: The amplitude zone plate. **(a)** An arbitrarily shaped 'mystery' device focuses incident radiation down to a spot at **P**. **(b)** An amplitude zone plate behaves just like this 'mystery' device in focusing incident radiation down to a spot at **P**. The dark areas of the zone plate serve to block out light which would otherwise destructively interfere at **P**, allowing for the constructive interference of all light at **P**.

Now let's journey back to the discussion concerning the yet-to-be-determined device illustrated in *Figure 3-1(a)*. The figure also depicts several dotted lines connecting different points on the device to **P**, representing paths traveled by the light in

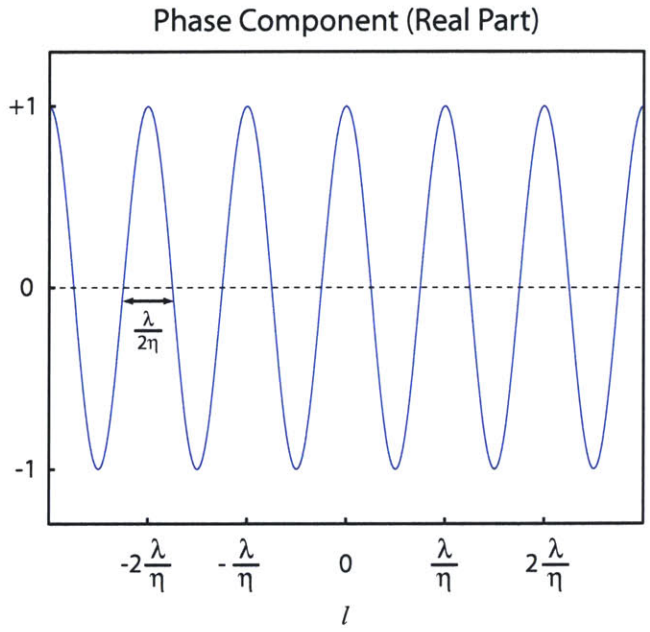

Figure 3-2: A plot of the real part of the phase component expressed in **Eq. 3-1**.

getting from the device to **P**. Light originating at precisely the midpoint of the device (black) exhibits some phase at **P**, be it positive or negative. For the sake of argument, let's say it's positive[1]. Then, light originating in close proximity to the midpoint of the device (blue) will also exhibit positive phases at **P**, since the differences in distance between their optical paths and the 'black' optical path are less than $\lambda/2\eta$. Light originating from these areas, therefore, constructively interfere with each other and with the light originating from the midpoint of the device, at **P**. However, as we move further away from the center of the device, a point will arrive where the light originating from that point (red) starts to exhibit negative phases at **P** and destructively interferes with the positive-phase light present at **P**. If we continue to move even further away from the center of the device, another point will arrive where the light originating from that point (blue) once again starts to exhibit positive phases at **P**. These sign changes are due to the periodicity of the phase component of light as discussed above, and will continue until the end of the device is reached.

We are now ready to unravel the mystery of a zone plate. A zone plate, which the mysterious device in *Figure 3-1(a)* portrays, does one of two things to ensure that no

[1] This is completely arbitrary and does not limit the outcome of the resulting analysis to this specific case.

light destructively interferes at **P**. It either blocks the destructive light (amplitude zone plate), or it alters the phase of the destructive light so that the light instead constructively interferes at **P** (phase zone plate). In addition, zone plates exhibit circular symmetry since all light originating from points on a circle centered on the zone plate's midpoint travel the same distance to get to **P**, and therefore possess the same phase at **P**. The concept of an amplitude zone plate is illustrated in *Figure 3-1(b)*.

3.2 Zone Plate Design

The intuitive theory presented above is sufficient for formulating the design of zone plates. Zone plates, in theory, either block or manipulate destructive light so that all light arriving at its focal point constructively interfere. For the time being let's focus on the blocking of destructive light, i.e. amplitude zone plates. Such zone plates are fabricated using highly absorbing materials such as gold (Au). *Figure 3-3* depicts the cross section of an amplitude zone plate. The dark and light colored regions represent, respectively, the presence and absence of Au. The locations of these regions are conveyed in the parameters $r_1, \ldots, r_n$. The design challenge, therefore, is to compute $r_1, \ldots, r_n$.

3.2.1 Computing $r_1, \ldots, r_n$:

First, recall that light travels a distance of $\lambda/2\eta$ before its phase changes sign (see *Figure 3-2*). Using this knowledge, we determine that light originating a distance r_1 from the center of the zone plate travels a distance of $f + \lambda/2\eta$ to get to **P**, where f represents the distance between the center of the zone plate and **P** (see *Figure 3-3*). Light originating a distance r_2 from the center of the zone plate travels a distance of $f + \lambda/\eta$ to get to **P**. Light originating a distance r_3 from the center of the zone plate travels a distance of $f + 3\lambda/2\eta$ to get to **P**. Continuing on, light originating a distance r_n from the center of the zone plate travels a distance of $f + n(\lambda/2\eta)$ to get to **P**. Note that in *Figure 3-3*, the odd subscripted radii, i.e. $r_1, r_3, r_5, \ldots$, represent the end of a light colored region and the beginning of a dark colored region while the even subscripted radii, i.e. $r_2, r_4, r_6, \ldots$, represent the end of a dark colored region and the beginning of a light colored region. For the remaining analysis, the term 'zone' is used in place of the term 'region.'

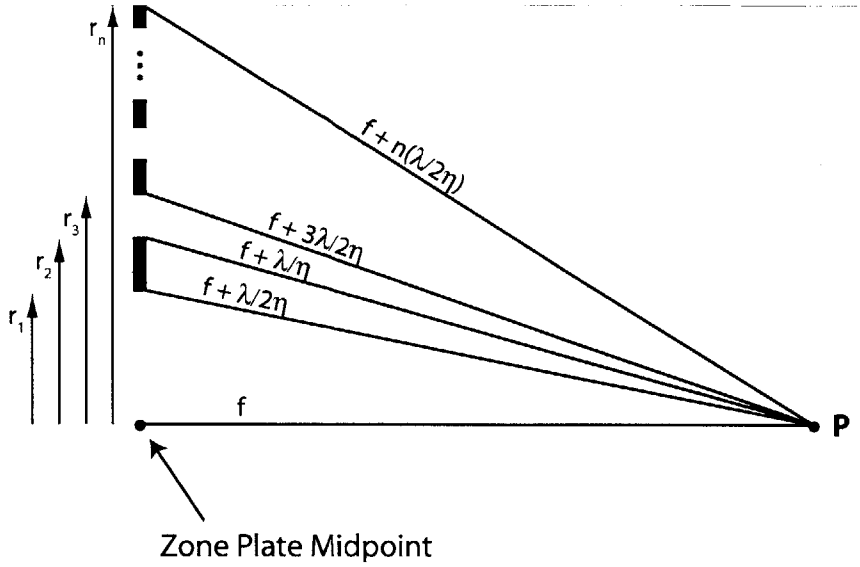

Figure 3-3: Zone plate geometry, illustrating the relationship between $r_1, \ldots, r_n$ and f, λ, η.

We equate the following terms using the Pythagorean Theorem:

$$r_n^2 + f^2 = \left(f + n\left(\frac{\lambda}{2\eta}\right)\right)^2 . \tag{3-2}$$

Rearranging terms in **Eq. 3-2** yields:

$$r_n = \sqrt{n\frac{\lambda f}{\eta} + n^2\frac{\lambda^2}{4\eta^2}} . \tag{3-3}$$

3.2.2 Remaining Zone Plate Design Steps

The following parameters are known or chosen prior to the design of a zone plate:

λ: The wavelength of the radiation source (λ = 400nm)

f: The focal length of the zone plate (f = 40μm)

NA: The numerical aperture of the zone plate (NA = 1.14)

η: The refractive index of the immersing medium ($\eta_{DI\text{-}water}$ = 1.34)

* Values chosen for our iZPAL experiments

NA is defined as:

$$NA = \eta \sin(\theta_{max}) = \eta \frac{R}{\sqrt{R^2 + f^2}}, \tag{3-4}$$

where θ_{max} is the physical convergence half-angle of the focused light, and R is the radius of the zone plate. Rearranging **Eq. 3-4** leads to the following formula for R:

$$R = f \frac{NA}{\sqrt{\eta^2 - NA^2}}. \tag{3-5}$$

N, the total number of zones in the zone plate, is found by substituting **Eq. 3-5** into **Eq. 3-3** (Note that N is an integer):

$$N = round\left[\frac{2\eta f}{\lambda}\left(-1 + \sqrt{1 + \frac{NA^2}{\eta^2 - NA^2}}\right)\right]. \tag{3-6}$$

To summarize, zone plates are designed in the following manner:

First, choose values for λ, f, NA, η.

Then, solve for N using **Eq. 3-6**.

Finally, solve for all r_n (from n = 1 to n = N) using **Eq. 3-3**.

3.2.3 Amplitude vs. Phase Zone Plates

The procedure described above, while intended for the design of amplitude zone plates, can also be applied to the design of phase zone plates. The only difference between the two zone plates is the material used for their fabrication. Amplitude zone plates use a highly absorbing material such as Au to block destructive light from reaching its focal point. Phase zone plates, instead of blocking destructive light, alter the destructive light's phase so that the light constructively interferes at its focal point. Phase zone plates are therefore fabricated using a non-absorbing material such as glass (SiO_2). The non-absorbing material used, however, cannot have a refractive index equal to that of the immersing fluid. The differing refractive indices are required for providing different phase shifts between the two mediums. *Figure 3-4* better illustrates this concept. Recalling the phase expression given in **Eq. 3-1**, the total phase shift experienced in materials 1 and 2 are respectively:

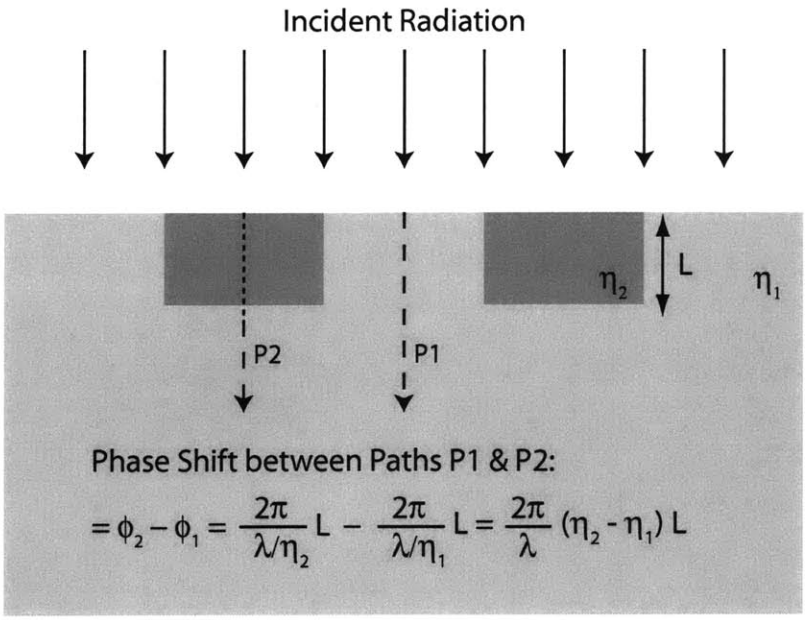

Figure 3-4: A depiction of the phase shift between light propagating in two different mediums. The effective wavelength of light propagating through a medium is dependent on the medium's refractive index. The phase shift is therefore dependent on the difference in the refractive indices of the two mediums.

$$e^{-i\left(\frac{2\pi}{\lambda/\eta_1}\right)L} \text{ and } e^{-i\left(\frac{2\pi}{\lambda/\eta_2}\right)L}, \tag{3-7}$$

where L is the thickness of the zone plate material, which in the case above corresponds to the thickness of material 2. The phase difference between light traveling in these two materials is therefore:

$$e^{-i\left(\frac{2\pi}{\lambda}(\eta_2-\eta_1)\right)L}, \tag{3-8}$$

and is varied by adjusting L. Introducing a π phase shift in the destructive light effectively makes it constructive. The thickness of the zone plate material needed for this π phase shift is:

$$L_{\pi-phase-shift} = \frac{\lambda}{2(\eta_2-\eta_1)}. \tag{3-10}$$

3.3 More Zone Plate Theory: Fourier Analysis

Now that the exact design of zone plates is known, a more rigorous analysis of these diffractive optical elements can be performed. Zone plates, both amplitude and phase, are designed using **Eq. 3-3**. For the case of short-wavelength low-NA zone plates, the '$n^2\lambda^2/4\eta^2$' term is negligible compared to the '$n\lambda f/\eta$' term and can be disregarded[2]. Then, r_n can be approximated by the following equation:

$$r_n \approx \sqrt{n\frac{\lambda f}{\eta}}. \tag{3-11}$$

3.3.1 Amplitude Zone Plates

The transmission function of an amplitude zone plate designed using **Eq. 3-11** is shown in *Figure 3-5*. Constructive light is completely transmitted while destructive light is completely blocked. Although the transmission function is not periodic, it can be made periodic by simply changing the abscissa from r to r^2. A periodic transmission function allows for it to be Fourier decomposed. An equation describing its behavior can be formulated from this decomposition, and is of the following form [21]:

$$t(\xi) = \sum_{n=-\infty}^{\infty} c_n e^{in\left(\frac{2\pi}{\Lambda}\right)\xi}. \tag{3-12}$$

where the coefficients, c_n, are computed by:

$$c_n = \frac{1}{\Lambda}\int_{\Lambda} t(\xi) e^{-in\left(\frac{2\pi}{\Lambda}\right)\xi} d\xi. \tag{3-13}$$

Plugging in the transmission function of an amplitude zone plate into **Eq. 3-13** yields:

$$c_n = \frac{1}{2}\mathrm{sinc}\left(n\frac{\pi}{2}\right). \tag{3-14}$$

Finally, substituting the resulting coefficients, **Eq. 3-14**, into **Eq. 3-12** yields an equation for the transmission function of an amplitude zone plate:

$$t(\xi) = \left[\frac{1}{2}\sum_{n=-\infty}^{\infty}\mathrm{sinc}\left(n\frac{\pi}{2}\right)e^{in\left(\frac{2\pi}{\Lambda}\right)\xi}\right]\cdot circ\left(\frac{\sqrt{\xi}}{R}\right). \tag{3-15}$$

[2] This is equivalent to saying $f >> n\lambda/4\eta$, which is true for short wavelengths and low NAs.

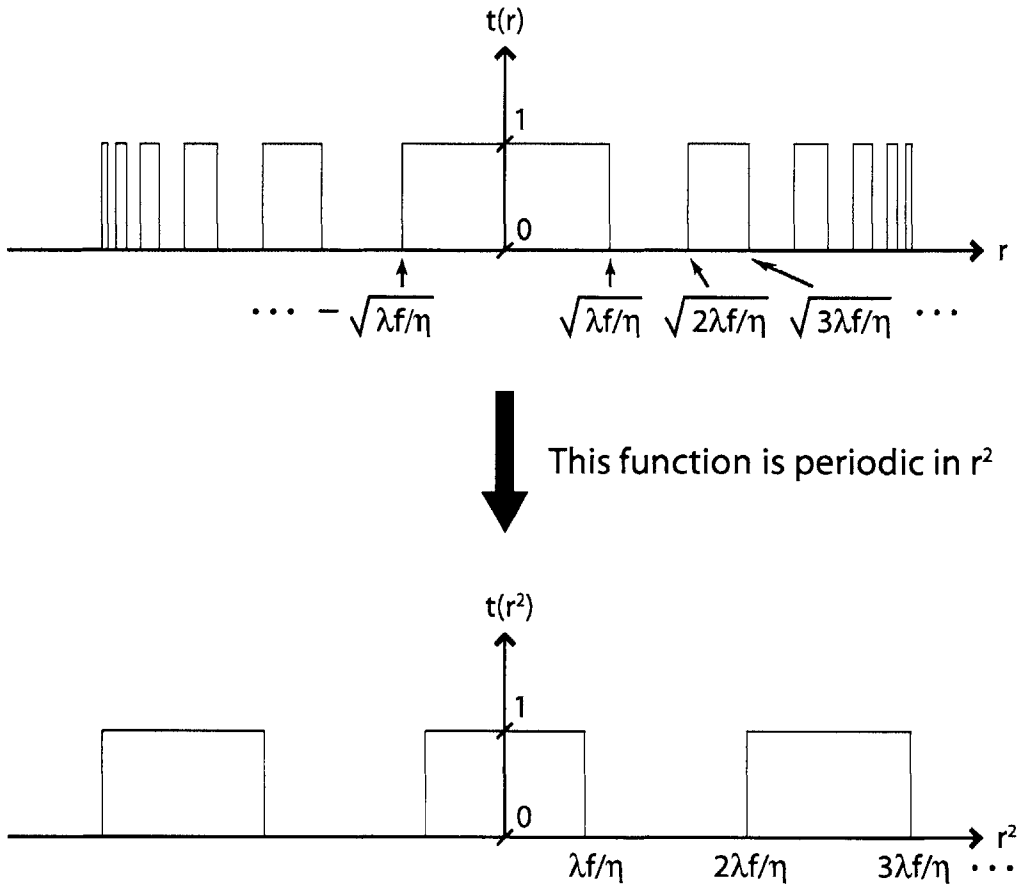

Figure 3-5: The transmission function of an amplitude zone plate. Notice that the transmission function is periodic in r^2.

Note that the added *circ* function gives the zone plate a finite size, i.e. a circle with radius R. Expanding this equation out, and substituting $\Lambda = 2\lambda f/\eta$, $\xi = r^2 = x^2 + y^2$ brings us to the following conclusions:

$$t(x,y) = \left[\frac{1}{2} + \frac{1}{\pi}e^{i\pi\frac{(x^2+y^2)}{(\lambda/\eta)f}} + \frac{1}{\pi}e^{-i\pi\frac{(x^2+y^2)}{(\lambda/\eta)f}} - \frac{1}{3\pi}e^{i\pi\frac{(x^2+y^2)}{(\lambda/\eta)(f/3)}} - \frac{1}{3\pi}e^{-i\pi\frac{(x^2+y^2)}{(\lambda/\eta)(f/3)}} + \ldots\right] \bullet \mathrm{circ}\left(\frac{\sqrt{x^2+y^2}}{R}\right) \qquad \textbf{(3-16)}$$

Plane wave (0^{th} diff. order)

Spherical wave focusing at z = +f (-1^{st} diff. order)

Spherical wave focusing at z = +f/3 (-3^{rd} diff. order)

Spherical wave diverging from z = -f (1^{st} diff. order)

Spherical wave diverging from z = -f/3 (3^{rd} diff. order)

The Fourier decomposition analysis presented above proves the diffractive focusing capabilities of amplitude zone plates. Fourier optics theory asserts that each term in **Eq. 3-16** (except for the constant term) describes a spherical wave. Not coincidently, these same spherical wave expressions are used to describe the output of refractive lenses subjected to plane wave inputs. We have, therefore, come full circle in demonstrating that amplitude zone plates focus light in a manner similar to conventional refractive optics. **Eq. 3-16** also reveals the multiple focal points of an amplitude zone plate, i.e. f, f/3, f/5, f/7, … *Figure 3-6* illustrates these focal points schematically. Of its infinite number of diffraction orders, the -1^{st} diffraction order, which carries the most intensity, is the one of most interest for lithography purposes. For amplitude zone plates, the -1^{st} diffraction order has a focusing efficiency of $1/\pi^2 \approx 10\%$.

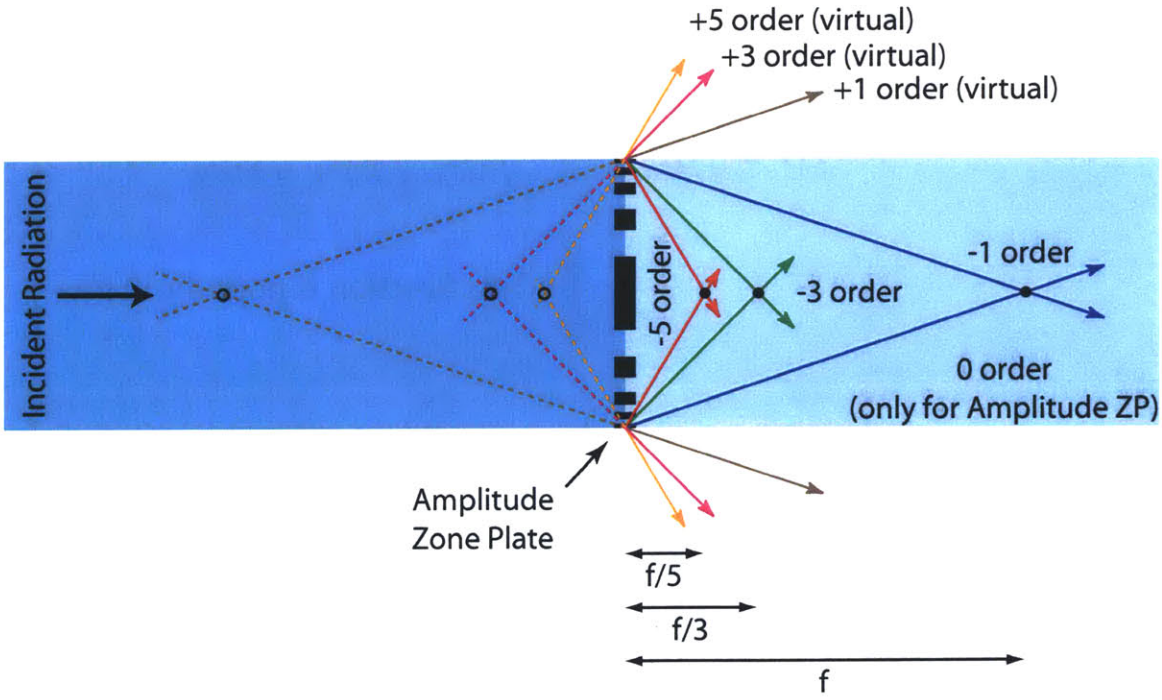

Figure 3-6: The multiple diffractive orders of an amplitude zone plate. Actually, this zone plate generates an infinite number of diffractive orders, even though only seven are depicted. One of these diffractive orders, the 0^{th} order, is not generated by phase zone plates.

3.3.2 Phase Zone Plates

We perform the same analysis for phase zone plates. The transmission function of a phase zone plate designed using **Eq. 3-11** is shown in *Figure 3-7*. Constructive light is unaltered while destructive light is π phase shifted, i.e. the sign of its phase is reversed. We again notice that the transmission function is not periodic, but can be made periodic by simply changing the abscissa from r to r^2, thus allowing it to be Fourier decomposed.

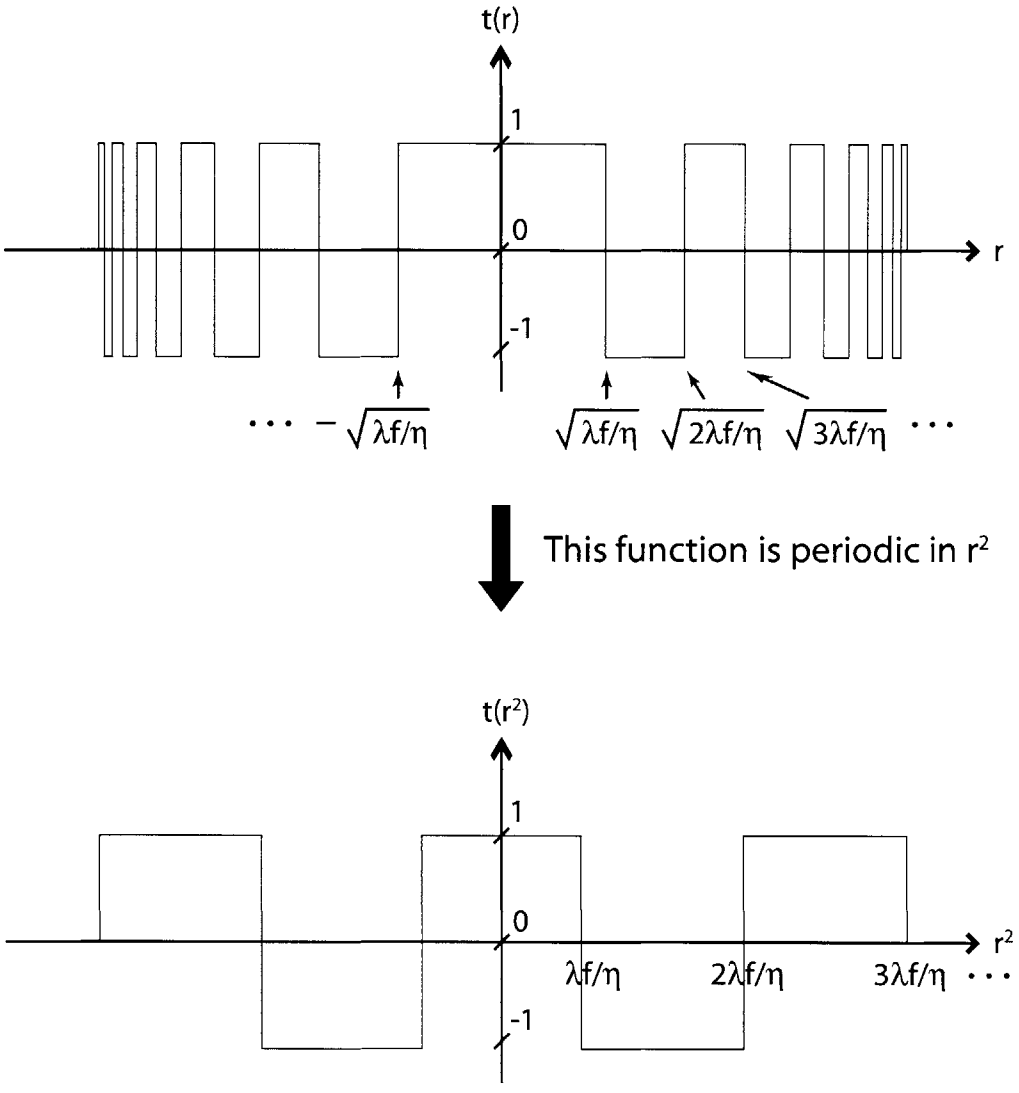

Figure 3-7: The transmission function of a phase zone plate. Notice that the transmission function is periodic in r^2.

The Fourier coefficients, c_n, are computed using **Eq. 3-13**. They are:

$$c_n = \begin{cases} \operatorname{sinc}(n\pi/2), & n \neq 0 \\ 0, & n = 0 \end{cases} \tag{3-17}$$

Plugging these coefficients, **Eq. 3-17**, into **Eq. 3-12** yields an equation for the transmission function of a phase zone plate:

$$t(\xi) = \left[\sum_{n=-\infty}^{-1} \operatorname{sinc}\left(n\frac{\pi}{2}\right) e^{in\left(\frac{2\pi}{\Lambda}\right)\xi} + \sum_{n=1}^{\infty} \operatorname{sinc}\left(n\frac{\pi}{2}\right) e^{in\left(\frac{2\pi}{\Lambda}\right)\xi} \right] \cdot circ\left(\frac{\sqrt{\xi}}{R}\right). \tag{3-18}$$

Expanding this equation out, and substituting $\Lambda = 2\lambda f/\eta$, $\xi = r^2 = x^2 + y^2$ leads to the following:

$$t(x,y) = \left[\frac{2}{\pi} e^{i\pi\frac{(x^2+y^2)}{(\lambda/\eta)f}} + \frac{2}{\pi} e^{-i\pi\frac{(x^2+y^2)}{(\lambda/\eta)f}} - \frac{2}{3\pi} e^{i\pi\frac{(x^2+y^2)}{(\lambda/\eta)(f/3)}} - \frac{2}{3\pi} e^{-i\pi\frac{(x^2+y^2)}{(\lambda/\eta)(f/3)}} + \ldots \right] \bullet \operatorname{circ}\left(\frac{\sqrt{x^2+y^2}}{R}\right) \tag{3-19}$$

Spherical wave diverging from z = -f (1st diff. order)

Spherical wave focusing at z = +f (-1st diff. order)

Spherical wave diverging from z = -f/3 (3rd diff. order)

Spherical wave focusing at z = +f/3 (-3rd diff. order)

Just as in the case of amplitude zone plates, the Fourier decomposition of a phase zone plate proves its diffractive focusing capabilities. The major difference between **Eq. 3-19** and **Eq. 3-16** is the absence of the 0^{th} diffraction order in the former. Its absence allows for the other diffraction orders to carry more intensity. Thus, the -1^{st} diffraction order in phase zone plates has a focusing efficiency of $4/\pi^2 \approx 41\%$, a four-fold improvement over amplitude zone plates.

3.4 Zone Plate Fabrication

Since phase zone plates possess much higher focusing efficiencies compared to amplitude zone plates, there's no reason not to use them over their amplitude counterparts for lithography. Therefore, this section will concentrate on the fabrication of phase zone

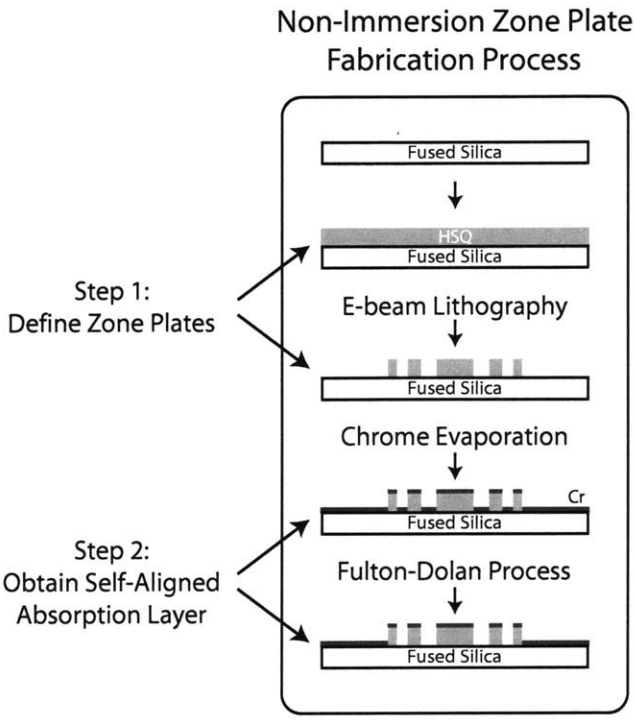

Figure 3-8: The two-step non-immersion zone plate fabrication process.

plates. Two different processes are described, one for the fabrication of non-immersion zone plates and the other for the fabrication of immersion zone plates.

3.4.1 The Non-Immersion Zone Plate Fabrication Process

Figure 3-8 illustrates a two-step process for the fabrication of non-immersion zone plates [22]. The zone plates themselves are actually defined in one exposure/development step. This simple, yet highly effective process for fabricating non-immersion zone plates would not be possible without a material known as Hydrogen Silsesquioxane (HSQ). HSQ was first developed by Dow Corning to serve as an inexpensive spin-on dielectric. A high temperature bake transforms the liquid spin-on dielectric into a material which closely resembles glass (SiO_2) in its properties. About a decade ago, it was discovered that HSQ could also double up as a negative e-beam resist [23]. It turns out that an e-beam exposure is equivalent to a high temperature bake as far as HSQ is concerned. HSQ's glass-like properties, i.e. a moderate refractive index relative to air and high

transparency to UV light, together with its sensitivity to electron beams makes it an ideal phase zone plate material.

A second step is needed to make the zone plates ready for ZPAL. Recall that ZPAL employs SST, which means that patterning is achieved through the exposure of discrete spots in a scanning manner. At any particular instance, the only radiation reaching the substrate should be radiation focused by the zone plates. However, since zone plates are circular in shape, there's no way an array of them can be oriented to cover the entire area of a zone-plate array. Therefore, there will always be illumination that is not incident on the zone plates. This radiation will pass through the zone-plate array unfocused and partially expose the underlying photoresist. To prevent this unwanted exposure, a layer of chrome (Cr) is placed in areas not covered by the zone plates[3]. *Figure 3-9* depicts the function served by this Cr layer.

Normally, the task-at-hand is achieved through an aligned exposure followed by a Cr-etch step. Fortunately for us, however, there is an easier approach. A process invented by Fulton and Dolan, appropriately named the Fulton-Dolan Process, can be used in place of the more difficult two-step process mentioned above to obtain an aligned Cr layer [24-25]. In fact, as we will explain shortly, this alignment between the Cr and the zone plates is perfect. The process is based on the principle of electrolysis, in which the etch rate of Cr is controlled by the voltage supplied to it. Another important observation needs to be made before we can explain our implementation of the Fulton-Dolan Process. It is the following: after a Cr evaporation, the Cr on top of the zone plates is nearly, if not entirely electrically isolated from the surrounding Cr layer. Now it is apparent how the Fulton-Dolan process is used to selectively control the etch rate of the surrounding Cr layer over the Cr on top of the zone plates. For our purposes, a positive voltage is applied to the surrounding Cr layer as it is immersed in a wet etchant, therefore severely reducing its etching compared to the etching of the Cr on top of the zone plates. In this manner, a self-aligned Cr layer can be created in all areas not covered by the zone plates.

[3] A 45nm thick layer of Cr is sufficient for blocking out more than 99% of the unwanted radiation (Cr has an absorbance coefficient of 3.56 at $\lambda = 400$nm).

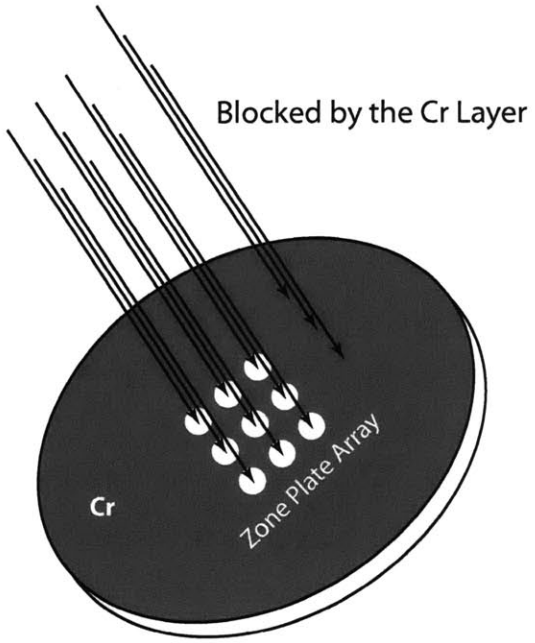

Figure 3-9: The purpose of the Cr layer for ZPAL. The Cr layer serves to block out all light not incident on the zone plates, thus ensuring that only light that passes through the zone plates reaches the substrate.

The HSQ/Fulton-Dolan process is a near optimal process for the fabrication of non-immersion zone plates. Both steps in the two-step process are generally easier to accomplish than their alternatives, yet produce better results. For instance, compare the one-step HSQ process to the more conventional exposure/liftoff/reactive-ion-etch (RIE) three-step process. Zone plates fabricated with the HSQ process exhibit less surface and sidewall roughness than those fabricated with the three-step process. Next, compare the Fulton-Dolan Process to the more conventional aligned exposure/etch two-step process. The former is not only easier, but produces a perfectly aligned Cr layer. Believe me, it's hard to do better than that.

Unfortunately, the HSQ/Fulton-Dolan process cannot be used for the fabrication of immersion zone plates. Recall that the refractive indices of the zone plate and immersion mediums cannot be identical; otherwise, a π phase shift cannot be introduced between adjacent zones. Although not identical, the refractive indices of HSQ and DI-water are so close that a zone height of 4μm would be needed to produce the π phase shift

(n_{HSQ} = 1.39, $n_{DI\text{-}water}$ = 1.34 at λ = 400nm)[4]. Considering that the outermost zones of zone plates are around 200nm in width, such high-aspect-ratio structures are extremely difficult to achieve with current nanofabrication processes.

3.4.2 The Immersion Zone Plate Fabrication Process

To avoid the high-aspect-ratio problem plaguing the HSQ process, a new process involving a higher index material was developed. Low-stress silicon nitride (SiN), with its high refractive index (n_{SiN} = 2.41 at λ = 400nm) and low absorption at 400nm wavelength light, is a good candidate. SiN, like SiO_2, is a very mature material, and as such, a great deal of research has been conducted for the optimization of its fabrication processes [26]. Using SiN as the zone plate material, a zone height of 187nm is all that's needed to produce the necessary π phase shift between adjacent zones.

3.4.2.1 Reflection Analysis

In addition to the requirement of a π phase shift, it is desirable to minimize the back reflection from the zone plate which now has three boundaries that produce reflections: SiO_2/H_2O, SiO_2/SiN, and SiN/H_2O. The SiO_2/H_2O interface has near zero reflectivity due to the small index mismatch. The following equation from electromagnetic theory for calculating reflections from multilayer planar surfaces, such as the one depicted in *Figure 3-10*, was used to approximate the total reflection, r, from the double boundary SiO_2/SiN/H_2O structure [20]:

$$r = \left| \frac{R_{01} + R_{12} e^{i2k_1 t_1}}{1 + R_{01} R_{12} e^{i2k_1 t_1}} \right|^2, \tag{3-20}$$

where k_m and t_m are the wavenumber and thickness of layer m, and R_{mn} is the reflection coefficient between layers m and n,

$$R_{mn} = \frac{k_m - k_n}{k_m + k_n}. \tag{3-21}$$

[4] A zone height of ~500nm is sufficient for providing the necessary π phase shift in the non-immersion case.

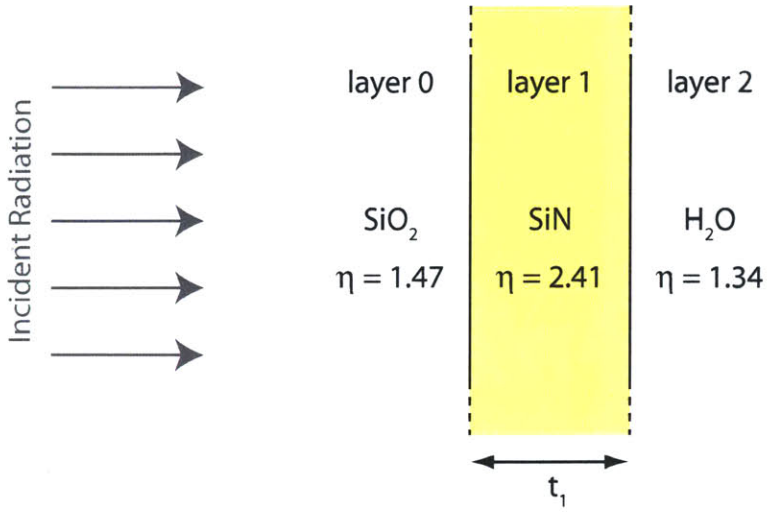

Figure 3-10: A planar three-layer (two-boundary) structure.

Figure 3-11 plots the reflectivity as a function of SiN thickness. From this plot, we observe that a SiN thickness of 166nm gives r < 1%, which is also close to the thickness needed to provide the π phase shift between adjacent zones (i.e. 187nm). Therefore, a SiN thickness of 166nm is used. To achieve the π phase shift between adjacent zones, an additional depth of 176nm is etched into the SiO_2 substrate.

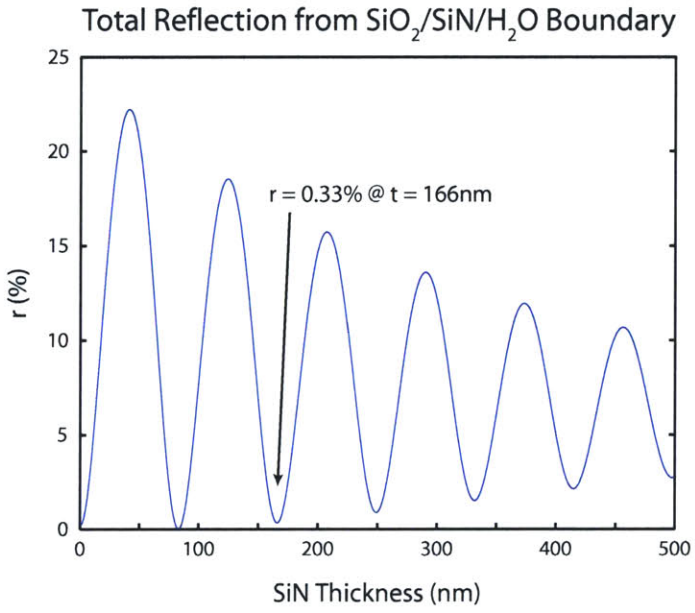

Figure 3-11: A plot of the total back-reflection from the medium depicted in *Figure 3-10*, as a function of SiN thickness. Notice that there are a number of local minima. For the fabrication of phase zone plates, the local minima corresponding to the SiN thickness closest to, without surpassing, the thickness needed for achieving a π phase shift between adjacent zones of a zone plate, is the one of relevance.

3.4.2.2 Fabrication Process

Figure 3-12 illustrates the process used for the fabrication of immersion zone plates. Note that the exposure/liftoff/RIE three-step process was employed. The liftoff and RIE steps were optimized so as to minimize the surface and sidewall roughness of the fabricated zone plates. Therefore, although the zone plates were fabricated using a more difficult process, their quality should be comparable to those fabricated with the HSQ process.

The immersion zone plate patterns are first exposed in Polymethyl Methacrylate (PMMA) resist using scanning-electron-beam lithography. Forward scattering and back

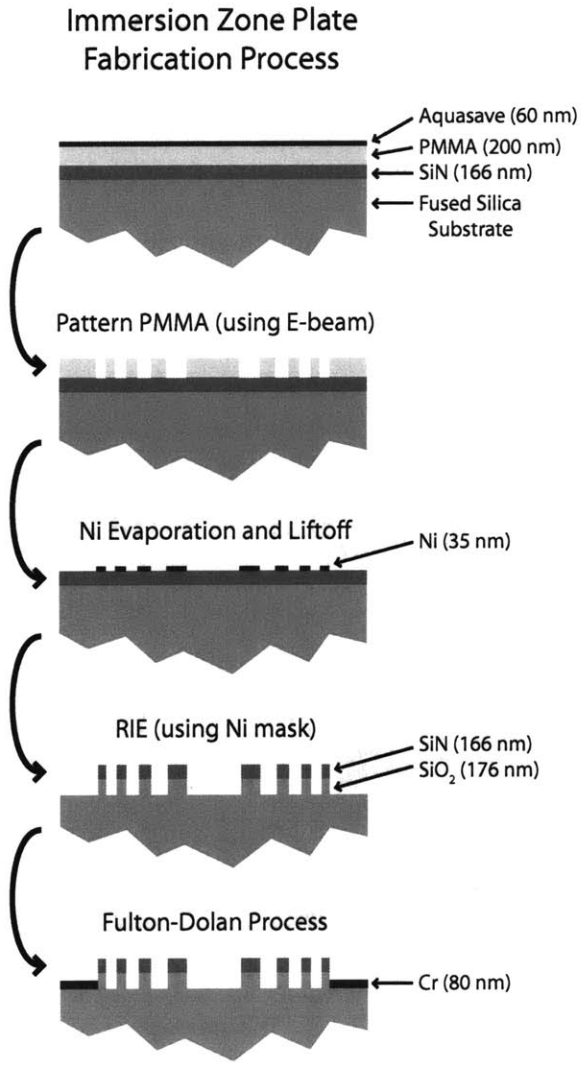

Figure 3-12: The immersion zone plate fabrication process.

reflection of the e-beam lead to the exposure of larger than intended feature sizes. Therefore, special care is taken to correctly bias the width of each individual zone so that the end result of an exposure is as close as possible to the intended pattern. A thin layer of Aquasave is spun on top of the PMMA to serve as a conductive layer for the exposure to prevent pattern distortions due to charging. The Aquasave is removed by a short DI-water rinse and subsequently, the PMMA is developed using a 2:1 IPA/MIBK mixture. The pattern is then transferred into nickel (Ni) using a liftoff process, followed by a RIE into the underlying SiN/SiO_2. The Ni etch mask is then removed using a standard Ni etchant. Finally, a thin layer of Cr is deposited over the entire substrate and the Fulton-Dolan Process used to selectively remove the Cr on top of the zone plates. The process is performed by connecting copper leads to the surrounding Cr layer while it is immersed in a Cr wet etchant. The voltage bias created by the contact of these two dissimilar metals is enough to inhibit the etching of the surrounding Cr layer. An optical micrograph illustrating a zone-plate array having undergone the above process is shown in *Figure 3-13*. The zone-plate array was illuminated from the bottom as the image was captured from above. Scanning-electron micrographs of a completed immersion zone plate are illustrated in *Figure 3-14*.

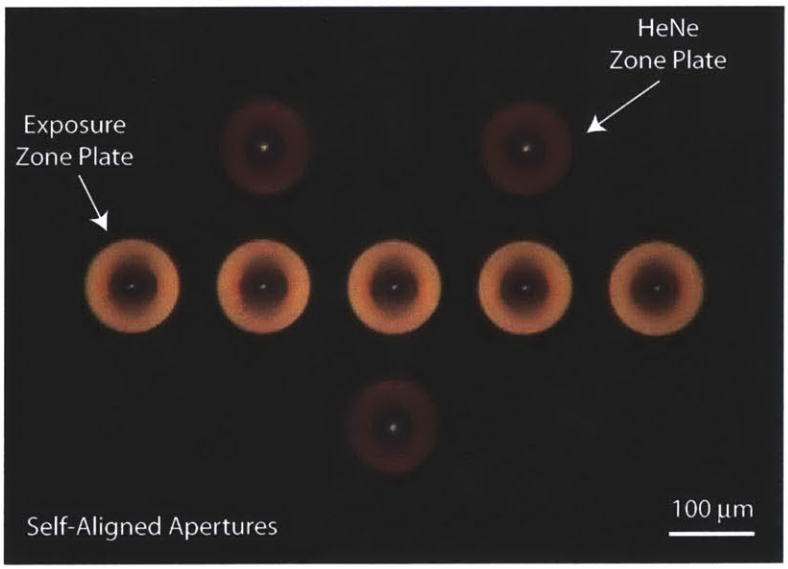

Figure 3-13: An optical micrograph of immersion zone plates fabricated using the process outlined in *Figure 3-12*. The micrograph also demonstrates the successful completion of the Fulton-Dolan Process. The zone-plate array is back-illuminated so only areas that are void of Cr (i.e. the immersion zone plates) pass light.

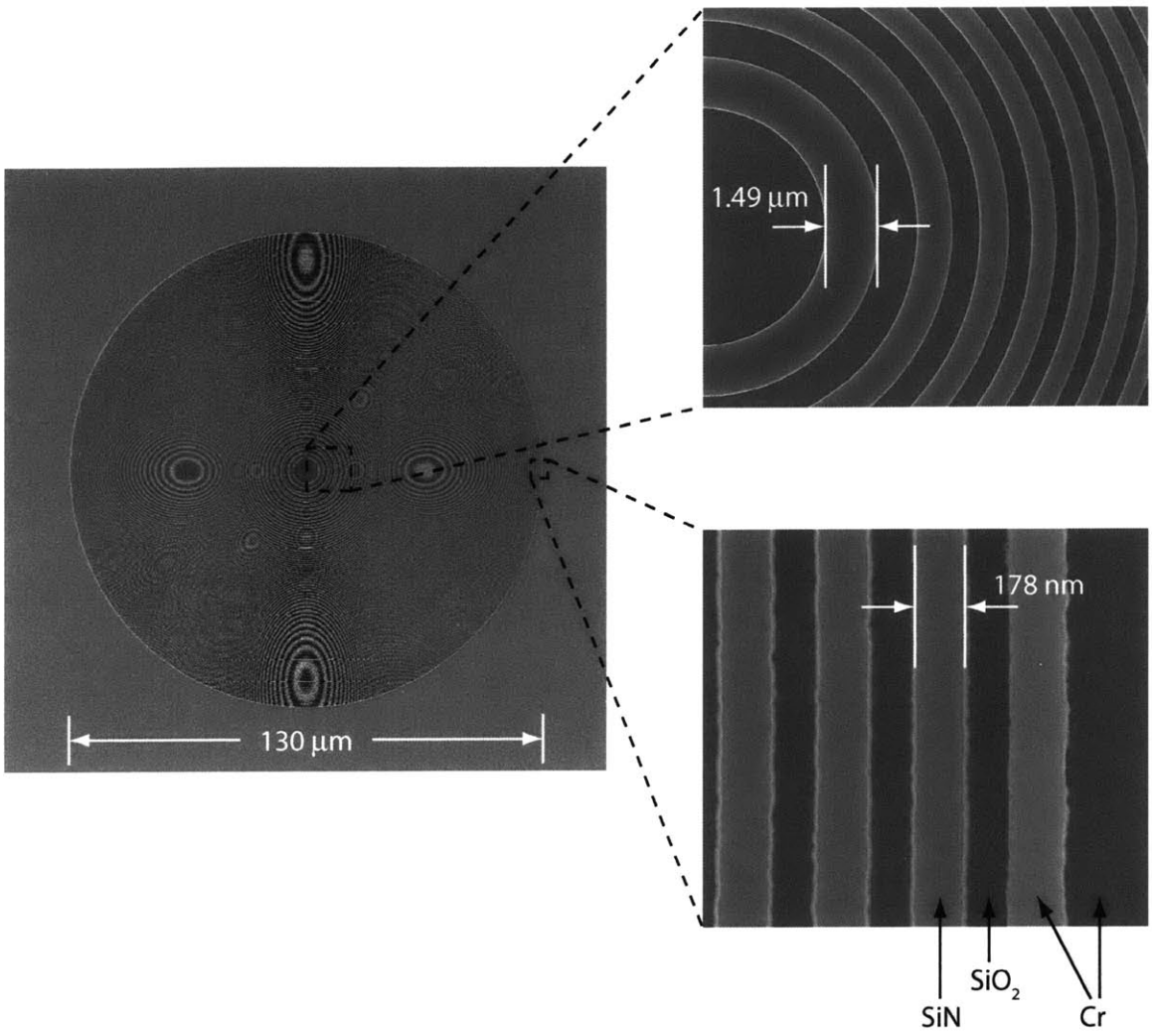

Figure 3-14: Scanning electron micrographs of a 1.14 NA immersion zone plate, designed for 400nm light. The moiré effect observed on the micrograph to the left is due to the sampling of the scanning electron microscope, and is not real.

Chapter 4

Zone Plate Characterization

From the very beginning it has been mentioned that a zone plate is a diffractive optical lens which can focus incident light down to a spot on its focal plane. This, however, does not tell the entire story. Naturally, the question arises... just how small is this spot? Is it infinitesimally small, or does it have some width? Actually, this question was answered implicitly in the previous chapter. The zone plate's transmission function, when expanded out, reveals that an infinitely small spot can theoretically be achieved with infinitely large zone plates. This, however, does not tell us much about the focusing capabilities of the more practical finite-sized zone plates. How well do such zone plates focus light? This will be explored in more detail in this chapter.

A zone plate's focusing ability is captured in its point-spread function (PSF), which denotes the intensity distribution of the focused light at the zone plate's focal plane. In addition to providing critical information regarding the sharpness of the focused radiation, the PSF also provides important information concerning sidelobes (i.e. local intensity peaks) and background radiation due to the other diffraction orders. All three affect the performance of SST-based lithography systems such as ZPAL, which expose discrete spots in a scanning manner. The PSF is therefore a good determinant of

the lithographic performance of such systems. Accurate knowledge of the PSF also enables the use of proximity-effect corrections (PEC) to adjust for both the sidelobes and background radiation [27].

We first take an analytical approach to solving for the zone plate's PSF. This approach requires information solved for in the previous chapter, which is only valid for short-wavelength low-NA zone plates. A more rigorous approach (which is not discussed here) is used for the simulation of higher NA zone plate PSFs. The results from these simulations are presented. Lastly, we characterize the zone plates used in our iZPAL experiments through the experimental reconstruction of their PSFs.

4.1 The Analytical Approach

The following analytical approach requires an equation for the zone plate's transmission function. However, such an equation has only been developed for short-wavelength low-NA zone plates. Therefore, the analysis presented below is only valid for the above stated case. We proceed with the transmission function provided from **Eq. 3-18**:

$$t(\xi)=\left[\sum_{n=-\infty}^{-1}\operatorname{sinc}\left(n\frac{\pi}{2}\right)e^{in\left(\frac{2\pi}{\Lambda}\right)\xi}+\sum_{n=1}^{\infty}\operatorname{sinc}\left(n\frac{\pi}{2}\right)e^{in\left(\frac{2\pi}{\Lambda}\right)\xi}\right]\cdot circ\left(\frac{\sqrt{\xi}}{R}\right), \qquad \textbf{(4-1)}$$

where $\Lambda = 2\lambda f/\eta$ and $\xi = x^2 + y^2$. Recall that the -1^{st} diffraction order carries the most intensity and is therefore the one utilized for lithography. The equation for the -1^{st} diffraction order is extracted from **Eq. 4-1**:

$$t_{n=-1}(x,y)=\frac{2}{\pi}e^{-i\pi\frac{x^2+y^2}{(\lambda/\eta)f}}circ\left(\frac{\sqrt{x^2+y^2}}{R}\right). \qquad \textbf{(4-2)}$$

The first part of this expression describes a spherical wave converging to a point a distance f from the zone plate, i.e. the focal plane of the zone plate. The total field at this plane, however, is not an infinitesimally small spot due to the second part of this expression. The Fresnel diffraction equation is used to solve for the total field:

$$g_{out}(x',y')=\frac{1}{i(\lambda/\eta)l}e^{i2\pi\frac{l}{(\lambda/\eta)}}\iint g_{in}(x,y)e^{i\pi\frac{(x'-x)^2+(y'-y)^2}{(\lambda/\eta)l}}dxdy, \qquad \textbf{(4-3)}$$

where (x,y) and (x',y') are the respective coordinates for the input and output planes, and l is the distance between these two planes [28]. In the present case, the input plane corresponds to the plane containing the zone plate and the output plane corresponds to the focal plane of the zone plate. Substituting $g_{in}(x,y) = t_{n=-1}(x,y)$ and $l = f$ into **Eq. 4-3** yields the following:

$$g_{out}(x',y') = \frac{1}{i\left(\lambda/\eta\right)f} e^{i2\pi\frac{f}{\left(\lambda/\eta\right)}} \iint \left[\frac{2}{\pi} e^{-i\pi\frac{x^2+y^2}{\left(\lambda/\eta\right)f}} circ\left(\frac{\sqrt{x^2+y^2}}{R} \right) \right] e^{i\pi\frac{(x'-x)^2+(y'-y)^2}{\left(\lambda/\eta\right)f}} dxdy$$

$$= \frac{2}{i\pi\left(\lambda/\eta\right)f} e^{i2\pi\frac{f}{\left(\lambda/\eta\right)}} e^{i\pi\frac{x'^2+y'^2}{\left(\lambda/\eta\right)f}} \iint circ\left(\frac{\sqrt{x^2+y^2}}{R} \right) e^{-i2\pi\left(\frac{x'}{\left(\lambda/\eta\right)f}\right)x - i2\pi\left(\frac{y'}{\left(\lambda/\eta\right)f}\right)y} dxdy$$

$$= \frac{2}{i\pi\left(\lambda/\eta\right)f} e^{i2\pi\frac{f}{\left(\lambda/\eta\right)}} e^{i\pi\frac{x'^2+y'^2}{\left(\lambda/\eta\right)f}} FT\left\{ circ\left(\frac{\sqrt{x^2+y^2}}{R} \right) \right\} \Bigg|_{u=\frac{x'}{\left(\lambda/\eta\right)f}, v=\frac{y'}{\left(\lambda/\eta\right)f}}$$

$$= \frac{2}{i\pi\left(\lambda/\eta\right)f} e^{i2\pi\frac{f}{\left(\lambda/\eta\right)}} e^{i\pi\frac{x'^2+y'^2}{\left(\lambda/\eta\right)f}} \left[\pi R^2 jinc\left(2\pi R \frac{\sqrt{x'^2+y'^2}}{\left(\lambda/\eta\right)f} \right) \right]$$

$$= \frac{2R^2}{i\left(\lambda/\eta\right)f} e^{i2\pi\frac{f}{\left(\lambda/\eta\right)}} e^{i\pi\frac{x'^2+y'^2}{\left(\lambda/\eta\right)f}} jinc\left(2\pi R \frac{\sqrt{x'^2+y'^2}}{\left(\lambda/\eta\right)f} \right). \qquad \textbf{(4-4)}$$

The PSF is therefore:

$$PSF = \left| g_{out}(x',y') \right|^2 = \frac{4R^4}{\left(\lambda/\eta\right)^2 f^2} jinc^2\left(2\pi R \frac{\sqrt{x'^2+y'^2}}{\left(\lambda/\eta\right)f} \right). \qquad \textbf{(4-5)}$$

The PSF of a short-wavelength low-NA zone plate computed using **Eq. 4-5** is plotted in *Figure 4-1*.

While the above analysis presents a nice closed form solution for the PSF of short-wavelength low-NA zone plates, it is more important that a method be developed to compute the PSF of high-NA zone plates, as these are more useful for lithography. A

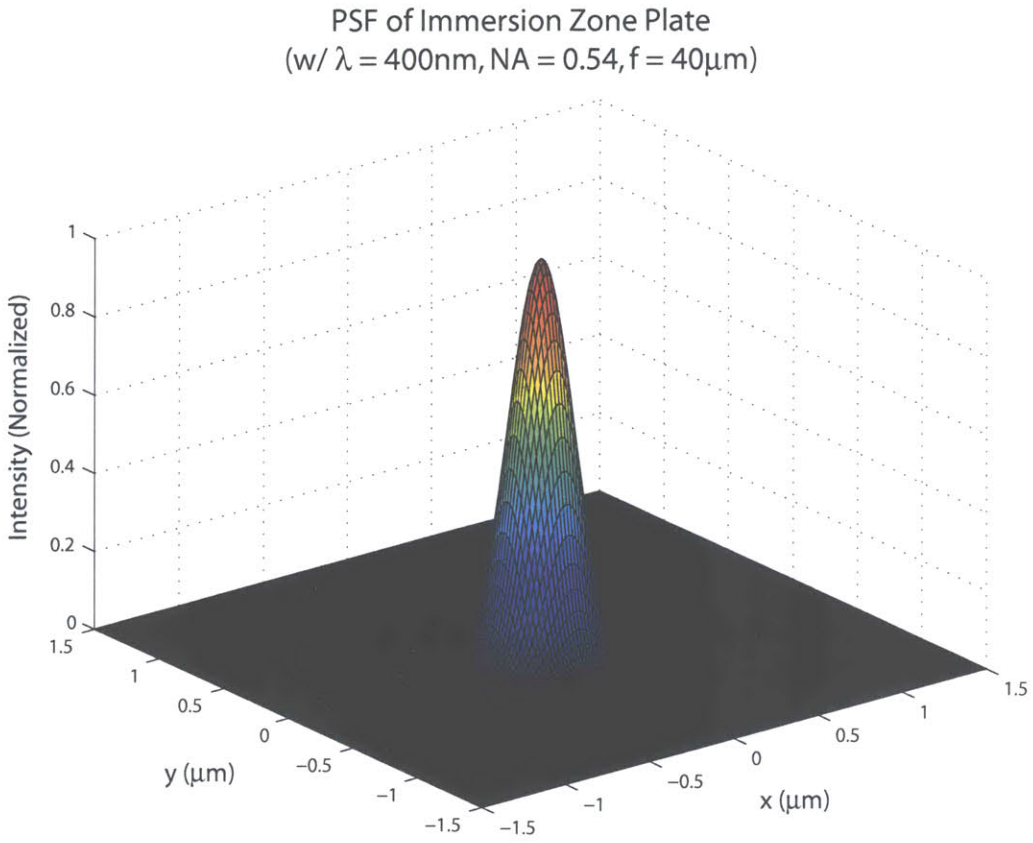

Figure 4-1: An approximate point-spread function of a 0.54 NA immersion zone plate computed with **Eq. 4-5**. For short wavelengths and low NAs, such as this, the approximation is fairly good.

rigorous electromagnetic model was developed by Rajesh Menon, another member of the ZPAL team, to do just this [13]. His method is not discussed here. However, his method is used to simulate the PSF of a 1.14 NA immersion zone plate. This simulated PSF is presented in *Figure 4-2*. The PSF of the same NA immersion zone plate is also computed using **Eq. 4-5** and plotted for comparison. Observe the nearly 50% error in spot-size between the two PSFs for high-NA zone plates.

4.2 The Experimental Approach

Figure 4-2 depicts the theoretical behavior of a 1.14 NA immersion zone plate. In other words, it depicts how such a zone plate is supposed to focus light at its focal plane. Do the zone plates used in our iZPAL experiments behave in this manner? To answer this

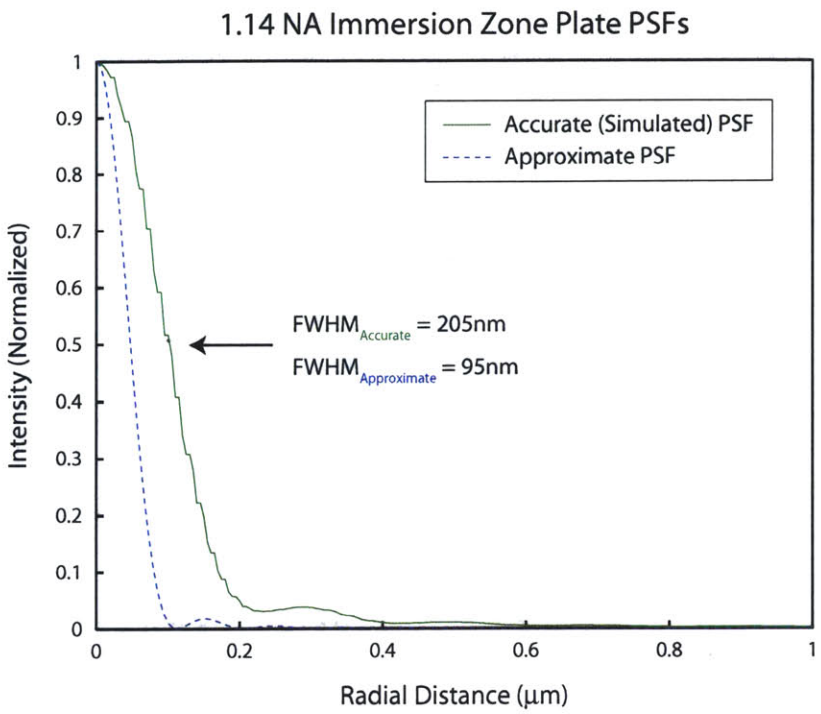

Figure 4-2: Accurate and approximate point-spread functions (PSFs) of a 1.14 NA immersion zone plate. The accurate PSF is simulated using a complex Finite-Difference-Time-Domain algorithm, while the approximate PSF is computed using **Eq. 4-5**. Notice that at high NAs, the approximation is no longer a good one.

question, a technique is developed to experimentally reconstruct the zone plates' PSFs [29]. The method calls for the exposure of discrete spots at a multitude of different doses. The resulting spot radii are then measured and used in conjunction with their corresponding doses to reconstruct the zone plate's PSF. The methodology is described in more detail below.

The PSF reconstruction methodology is better explained with *Figure 4-3*. As mentioned in this chapter's introduction, the PSF signifies the intensity distribution of the focused light at the zone plate's focal plane (see *Figure 4-3(a)*). The distribution of dose received by the photoresist, D(r), is related to the intensity distribution, I(r), by the following:

$$D(r) = I(r) \times t, \qquad \textbf{(4-6)}$$

where t represents the total time of exposure.

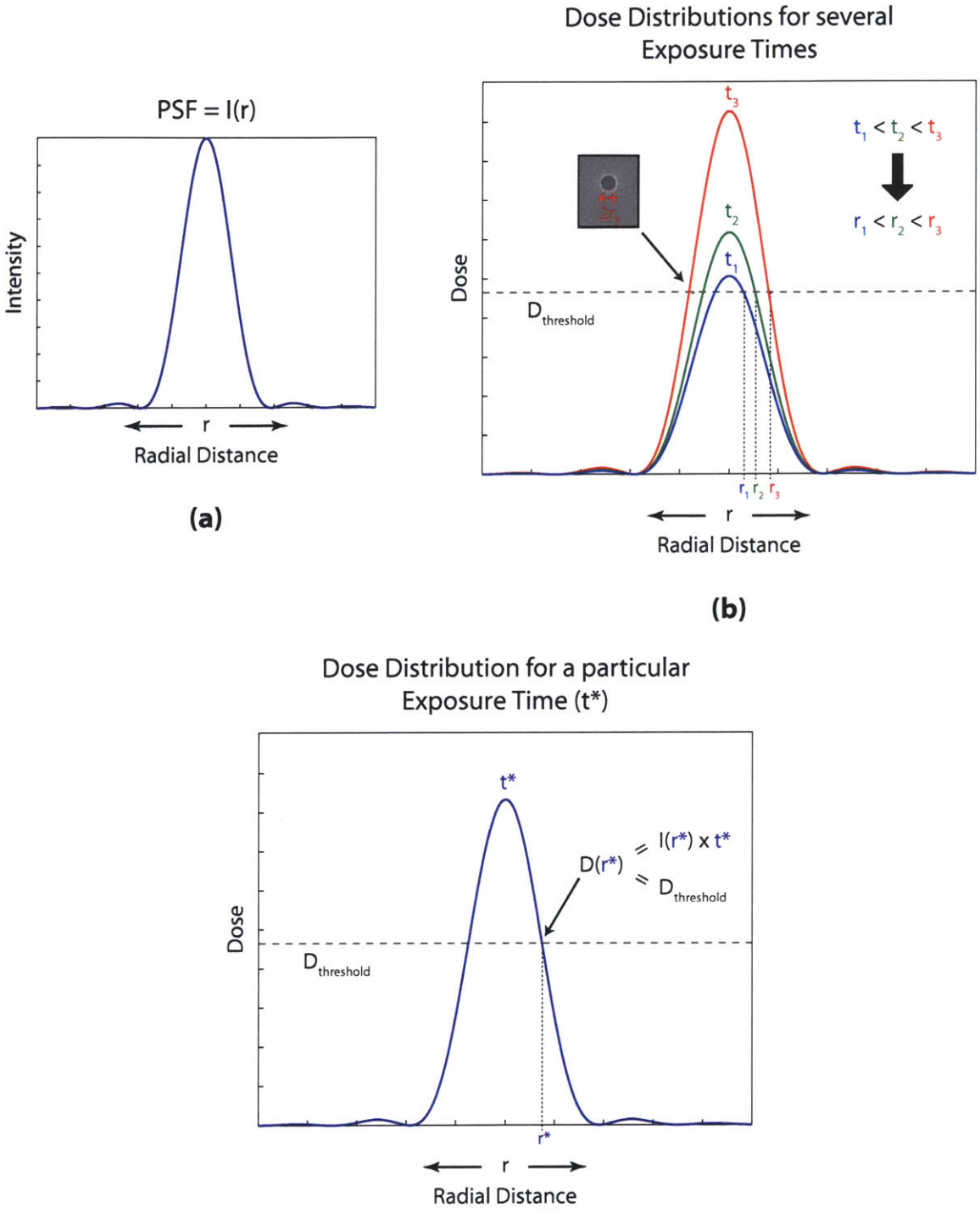

Figure 4-3: The point-spread function (PSF) reconstruction process. **(a)** A zone plate's PSF represents the intensity distribution at the zone plate's focal plane. **(b)** Dose distributions for several exposure times. Note that areas of a positive photoresist receiving doses greater than $D_{threshold}$ are removed during the development process. **(c)** A dose distribution for a particular exposure time t^*. The relationship between the PSF at $r = r^*$, i.e. $I(r^*)$, and t^* is illustrated.

Figure 4-3(b) depicts D(r) at several exposure times. For a particular exposure time t^*, a spot with radius r^* is formed in the photoresist. The relationship between the parameters t^* and r^* is illustrated in *Figure 4-3(c)*. It is:

$$I(r^*) \times t^* = D_{threshold}\,. \tag{4-7}$$

Rearranging **Eq. 4-7** yields the value of the PSF at $r = r^*$:

$$PSF(r^*) = I(r^*) = \frac{D_{threshold}}{t^*}\,. \tag{4-8}$$

Therefore, each (t^*, r^*) dataset determines one point of the PSF. More points are found by exposing additional spots at different exposure times. The resulting spot radii and their corresponding exposure times are then used to reconstruct the zone plate's PSF. The constant valued $D_{threshold}$ is determined by normalization of the reconstructed PSF to the theoretical PSF.

Note that this technique assumes the photoresist possesses infinite contrast. In other words, the photoresist is assumed to behave in a binary manner such that areas of the photoresist receiving doses less than $D_{threshold}$ are considered unexposed while areas of the photoresist receiving doses greater than or equal to $D_{threshold}$ are considered exposed (see *Figure 4-4*). This is a reasonable assumption considering most positive photoresists exhibit highly nonlinear behavior.

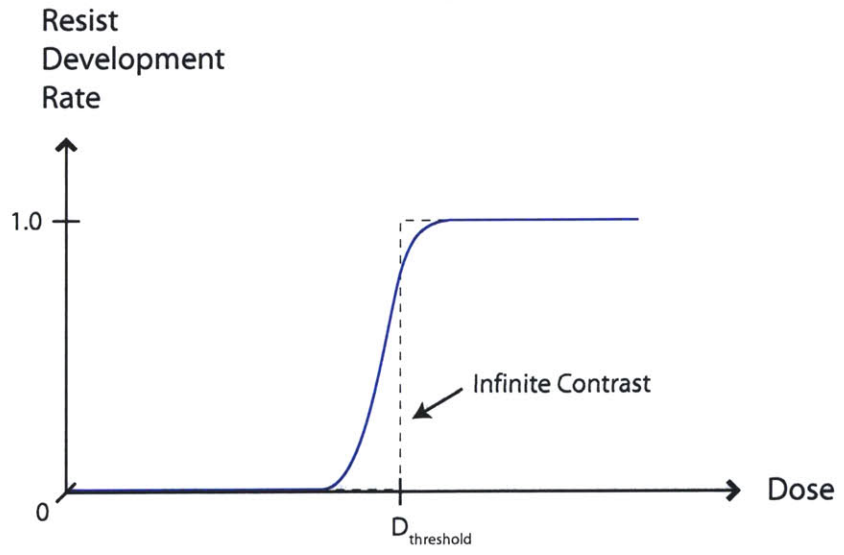

Figure 4-4: Typical nonlinear behavior of positive photoresists.

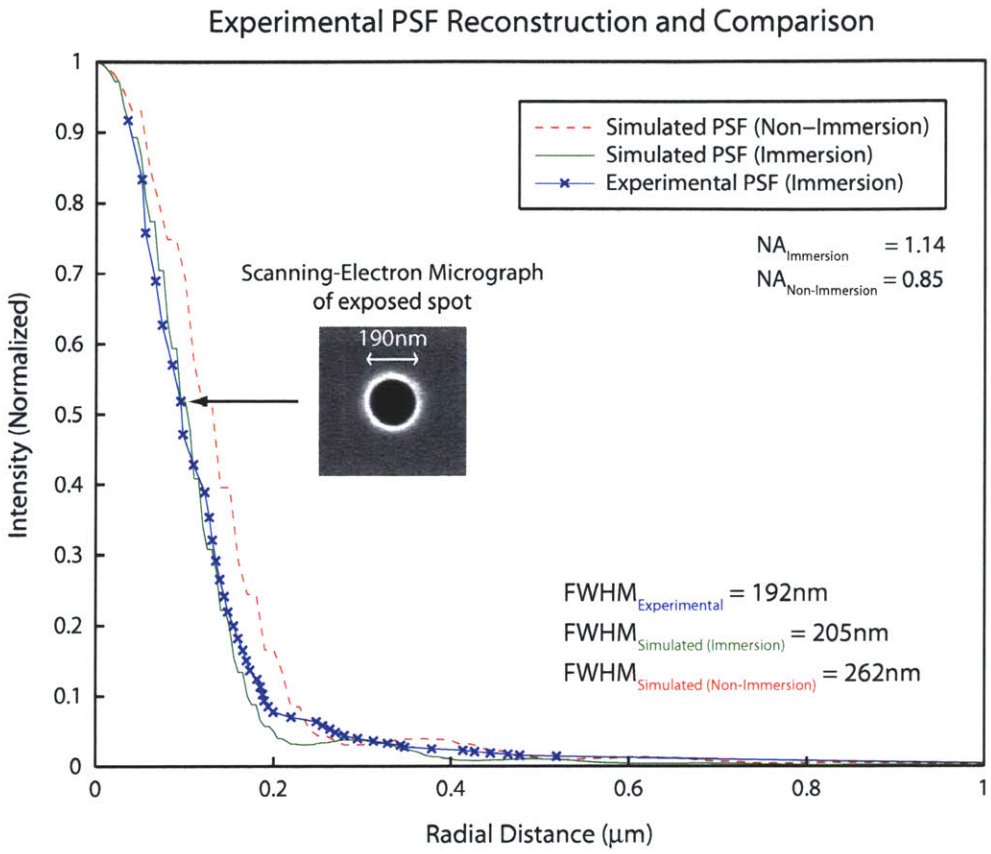

Figure 4-5: Comparison between the experimental and theoretical immersion and non-immersion zone plate point-spread functions (PSFs). There is close agreement between the experimental and theoretical immersion PSFs, as their spot-sizes are within 6% of one another (195nm vs. 205nm). Furthermore, the spot-size of the immersion PSF is smaller than the spot-size of the non-immersion PSF by a factor of 1.36, which agrees well with the expected factor of 1.34 ($\eta_{DI\text{-}water}$).

4.3 Characterization of Immersion Zone Plates

The PSF of a 1.14 NA immersion zone plate is experimentally reconstructed following the procedure outlined above, and is plotted in *Figure 4-5* along with theoretically simulated PSFs for an immersion and non-immersion zone plate. The reconstructed PSF (blue) is first compared to the simulated PSF of an immersion zone plate (green). It is observed that the PSFs agree well with one another. To be more quantitative, we define the zone plate's spot-size as the full-width-at-half-maximum (FWHM) of its PSF, and see that the spot-size of the reconstructed PSF (192nm) is only 6% smaller than the spot-size

of the simulated PSF (205nm). The reconstructed PSF (blue) is next compared to the simulated PSF of a non-immersion zone plate (red)[1]. In this case, the spot-size of the reconstructed PSF is a factor of 1.36 smaller than the spot-size of the simulated PSF (262nm). This decrease in spot-size leads us to expect a similar increase in iZPAL's lithographic performance, which is the subject of the next chapter.

[1] The non-immersion zone plate being compared has an NA of 0.85

Chapter 5

iZPAL System Performance

Does the immersion scheme really work? If the previous chapter has any say, then the answer is yes. In that chapter, the scheme demonstrated a marked improvement in the focusing abilities of the zone plates. This would lead us to believe and expect that a similar improvement in ZPAL's lithographic performance is feasible.

What exactly is meant by the lithographic performance of a lithography system? Obviously, the system's resolution, i.e. how small it can reliably print, is a key component. This, however, is not the only important component to a lithography system. Does it matter how small a system can print, if the slightest variation in its dose causes a complete under or overexposure? Does it matter how small a system can print, if the slightest shift in its focus leads to total pattern washout? Thus, the exposure latitude and depth-of-focus of a lithography system are also key contributors to the system's overall performance. All three properties will be examined in assessing the performance of immersion ZPAL compared to non-immersion ZPAL.

5.1 Resolution

The resolution of a lithography system indicates the smallest feature size the system can print reliably. The term 'reliably' is important to the definition because a system rated as having 10nm resolution should be able to print 10nm lines spaced 10nm apart. Often times, a thin isolated feature is used to claim high resolution patterning. Such thin isolated features can be achieved using a number of 'tricks' and therefore does not determine the resolution of the patterning system. A more accurate representation of a system's resolution is determined through the patterning of dense lines and spaces at that resolution.

For optical lithography, this resolution is expressed by the following equation:

$$W_{\min} = k_1 \frac{\lambda}{NA}, \tag{5-1}$$

where W_{min} represents the minimum linewidth of a dense line/space pattern, k_1 is a proportionality constant which takes into account various system and non-system variables such as system non-idealities, resist clipping properties, and environmental conditions, λ is the wavelength of the radiation, and NA is the numerical aperture of the optical system defined as:

$$NA = \eta \sin(\theta_{\max}), \tag{5-2}$$

where θ_{max} is the physical convergence half-angle and η is the refractive index of the medium between the last optical element (e.g. the zone-plate array) and the substrate. Hence, introducing a medium with $\eta > 1$ between the zone-plate array and the substrate increases NA by a factor of η, and as a consequence, decreases W_{min} by the same factor of η. This is the essence of the immersion scheme.

The non-immersion ZPAL system has achieved W_{min} as low as 135nm with the following parameters: $k_1 = 0.29$, $\lambda = 400$nm, NA = 0.85 [30] (see *Figure 5-1*). Increasing the NA using the immersion scheme with DI-water as the immersion medium ($\eta_{DI\text{-}water} = 1.34$ at $\lambda = 400$nm) should therefore allow W_{min} as low as 100nm to be theoretically achievable[1]. To date, dense lines/spaces with linewidths as low as 115nm have been

[1] This assumes the same values for k_1 (= 0.29) and λ (= 400nm) obtained with the non-immersion system.

successfully patterned with the immersion scheme (see *Figure 5-2*), which is a significant improvement in resolution over the non-immersion scheme.

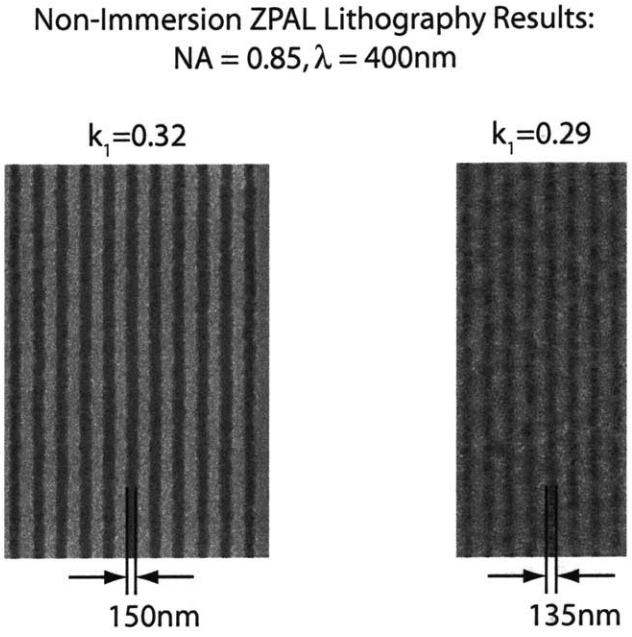

Figure 5-1: Dense lines and spaces patterned with ZPAL. The 135nm lines/spaces is its highest demonstrated resolution.

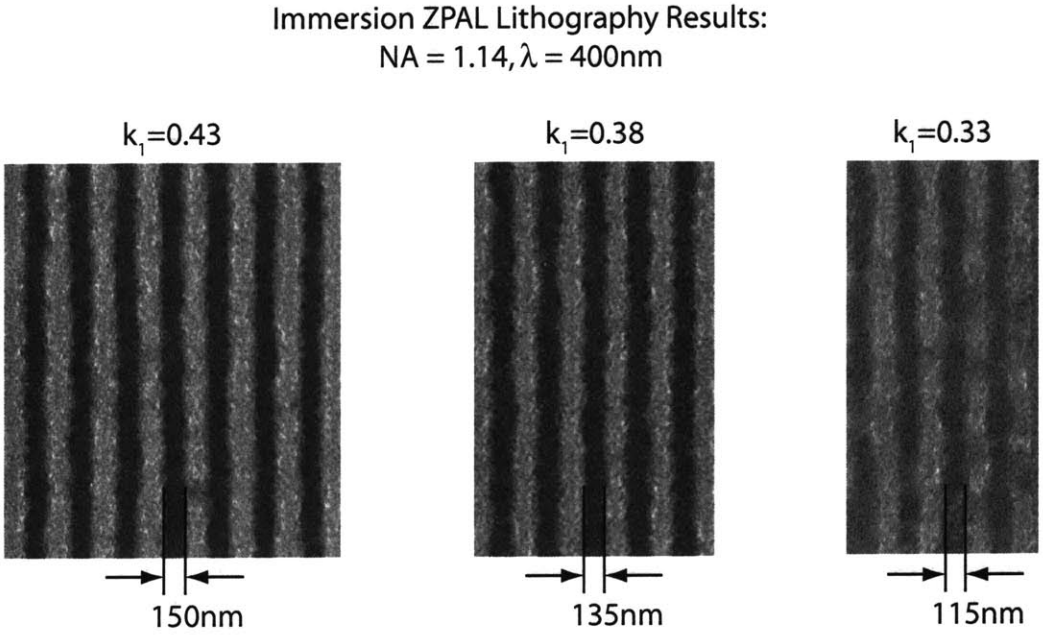

Figure 5-2: Dense lines and spaces patterned with iZPAL. The 115nm lines/spaces is its highest demonstrated resolution.

To be quantitative, the immersion scheme improved resolution by a factor of 1.17, not 1.34 as theoretically speculated. The inability to print down to the theoretical minimum linewidths is most likely due to a decrease in the diffractive efficiency of the zone plates. This effect was observed in our experiments as higher doses (exposure times) were needed for the immersion exposures. The reason for this drop in diffractive efficiency, however, is still not yet well understood. Could the DI-water, which is one of the few major differences between the immersion and non-immersion systems, be at fault? Admittedly, due to the lack of available means, the value for $\eta_{DI\text{-}water}$ was taken from literature instead of being experimentally measured. Since the immersion zone plates were designed with this value in mind, any variation to $\eta_{DI\text{-}water}$ leads to non-π phase shifts between adjacent zones of the zone plates, resulting in lower diffractive efficiencies for the zone plates. This was a concern from the very beginning. Therefore, if this is indeed the problem, a solution for it has been identified and is presented in the next chapter. Whatever the cause may be, one thing is certain. The drop in the immersion zone plate's diffractive efficiency leads to a reduction in image contrast, making it hard to achieve the theoretically stipulated resolution levels.

The immersion scheme provides another advantage over the non-immersion scheme. For a particular resolution, the immersion scheme prints higher quality patterns, i.e. higher pattern fidelity, compared to the non-immersion scheme. The reasons for this are better explained from a quantitative point of view. For that, we reintroduce the k_1 parameter. k_1 is a proportionality constant in **Eq. 5-1**, which in some respects can be viewed as the difficulty level for printing at a certain resolution. This makes intuitive sense as patterns become harder and harder to print at decreasing linewidths, i.e. at decreasing k_1. Generally, the quality of a pattern is correlated to its difficulty in printing (k_1) as is evidenced in both *Figure 5-1* and *Figure 5-2*. We are now prepared to compare the immersion and non-immersion schemes with regard to pattern fidelity at the same resolutions, using k_1 as a measuring stick. 135nm lines/spaces printed with the non-immersion scheme correspond to a k_1 of 0.29, while the same resolution lines/spaces printed with the immersion scheme correspond to a k_1 of 0.38. Just by comparing the values for k_1 leads us to conclude that 135nm lines/spaces are easier to print with the immersion scheme, and is thus printed with higher pattern fidelity using this scheme.

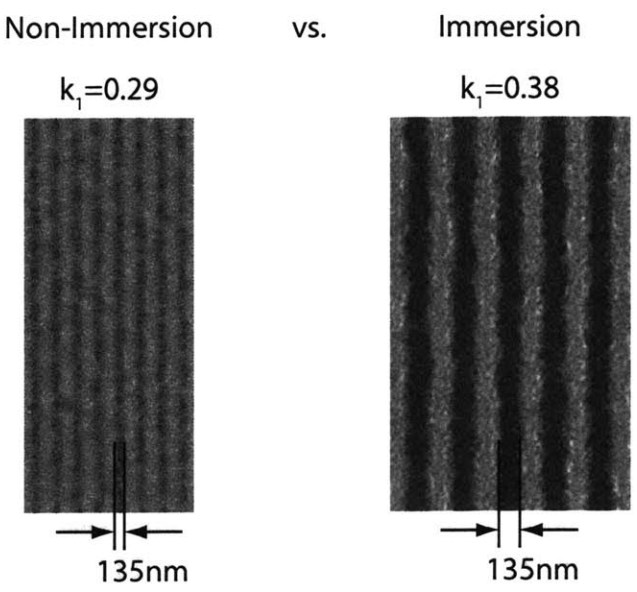

Figure 5-3: Comparison between 135nm dense lines/spaces patterned with both ZPAL and iZPAL. The immersion exposure clearly exhibits better pattern fidelity.

This is evidenced in *Figure 5-3*, which illustrates 135nm lines/spaces printed with both schemes.

5.2 Exposure Latitude and Depth-of-Focus (DOF)

The exposure latitude and DOF for a lithography system represent, respectively, the range of doses and foci from the optimal dose and focus which lead to only insubstantial changes in exposed feature sizes. Insubstantial in this context usually refers to under 10%. Equations for both the exposure latitude and DOF are intentionally left out of this thesis. The author feels that these equations are both confusing and misleading, and therefore do not add much to the discussion. For instance, the author knows of three (there are probably more) different versions of the DOF equation, each for its own particular circumstance. Instead, an intuitive argument is presented and experiments performed to demonstrate its validity. In other words, we let the experimental results do the talking.

It makes sense intuitively, that the immersion scheme improves both the exposure latitude and DOF of a lithography system. It was mentioned above that at any particular

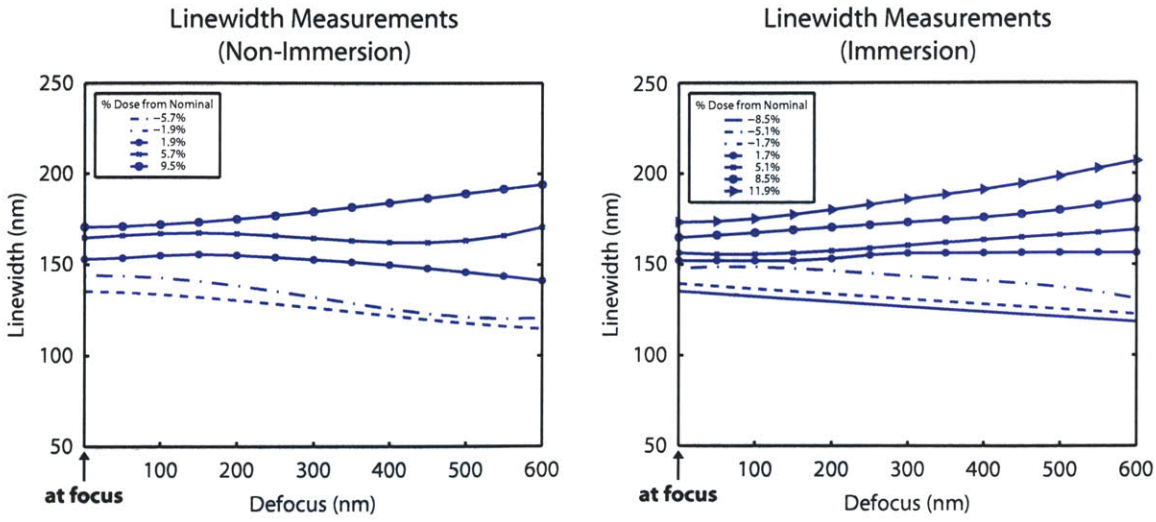

Figure 5-4: Plots of exposed linewidths measured over a range of dose and defocus for both ZPAL and iZPAL.

resolution, $k_{1,\ immersion} > k_{1,\ non\text{-}immersion}$, meaning that for any particular resolution, patterns at that resolution are easier to print with the immersion scheme. At least part of the reason for this has to be due to increases in exposure latitude and DOF with the immersion scheme.

Generally, a plot of the exposure window is more useful than the exposure latitude and DOF values themselves. The exposure window represents the different combinations of dose/focus variations from their optimal values such that only insubstantial changes are observed in the exposed feature sizes. Therefore, the larger the window, the more room for error the system can tolerate. We define the exposure window quantitatively to be the range of dose and defocus values which produce linewidths that vary less than ±5% from the nominal linewidth (critical dimension). To experimentally determine this exposure window, dense 150nm lines/spaces were first patterned over a wide range of dose and defocus values. The linewidth of the center of the exposed region for each 150nm line/space is subsequently measured and plotted as a function of both dose and defocus values (see *Figure 5-4*). For both the immersion and non-immersion schemes, the linewidths are close to the nominal value (150nm) at focus and become further and further spaced apart with increasing defocus. This decrease in

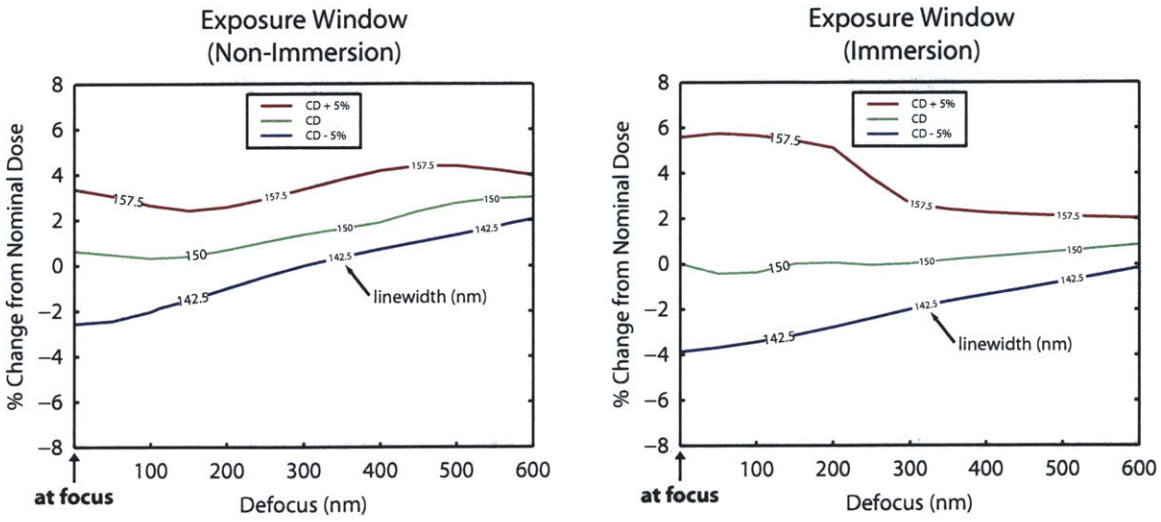

Figure 5-5: Exposure window plots. Linewidth data from *Figure 5-4* is extrapolated to find the dose/defocus combinations needed to print at the critical dimension (150nm), CD + 5% (157.5nm), and CD - 5% (142.5nm). The area between the CD + 5% and CD - 5% curves defines the exposure window, which is clearly larger for the immersion system.

exposure latitude for increasing defocus is less severe for the immersion system as compared to the non-immersion system, indicating a larger exposure window.

The linewidth data plotted in *Figure 5-4* is then used to extrapolate exposure windows for both immersion and non-immersion schemes (see *Figure 5-5*). Contours of linewidths equal to 150nm, 150nm + 5%, 150nm – 5% are shown as a function of dose and defocus. A larger exposure window is clearly observed for the immersion scheme. Moreover, at focus, the immersion scheme possesses an exposure latitude of ~9.5% compared to only ~5.9% for the non-immersion scheme. In addition, the exposure window for the immersion system remains fairly constant for defocus values up to ~200nm compared to a more rapid decrease in the exposure window for the non-immersion system.

5.3 Additional Lithography Results

Up to this point, only dense lines/spaces lithographic patterns have been presented. These patterns are sufficient for demonstrating our case for immersion lithography, but a

case also needs to be made for maskless lithography as iZPAL is an immersion maskless lithography system. For this reason, we present the following patterns exposed with iZPAL. *Figure 5-6* shows 150nm and 190nm dense nested-L's, which are a variant of the dense lines/spaces pattern. Patterning lines/spaces in both the horizontal and vertical directions enables the measurement of astigmatism in the focused radiation spot. *Figure 5-7* shows a 150nm and 190nm-spaced array of holes. Such an array has numerous applications ranging from two-dimensional photonic crystals to contact holes for connecting multi-layered devices. The next (and last) pattern truly exemplifies the maskless approach. *Figure 5-8* depicts the official logo of the Electron, Ion, and Photon Beam Technology and Nanofabrication (EIPBN) conference 2005. The author presented a poster at this conference and felt that such a pattern would illustrate the power of immersion maskless lithography. Such a pattern would probably never be realized in a mask-based lithography system. While 'cute', this pattern is by no means worth the cost of the mask needed to produce it. Luckily for the author, iZPAL is maskless!

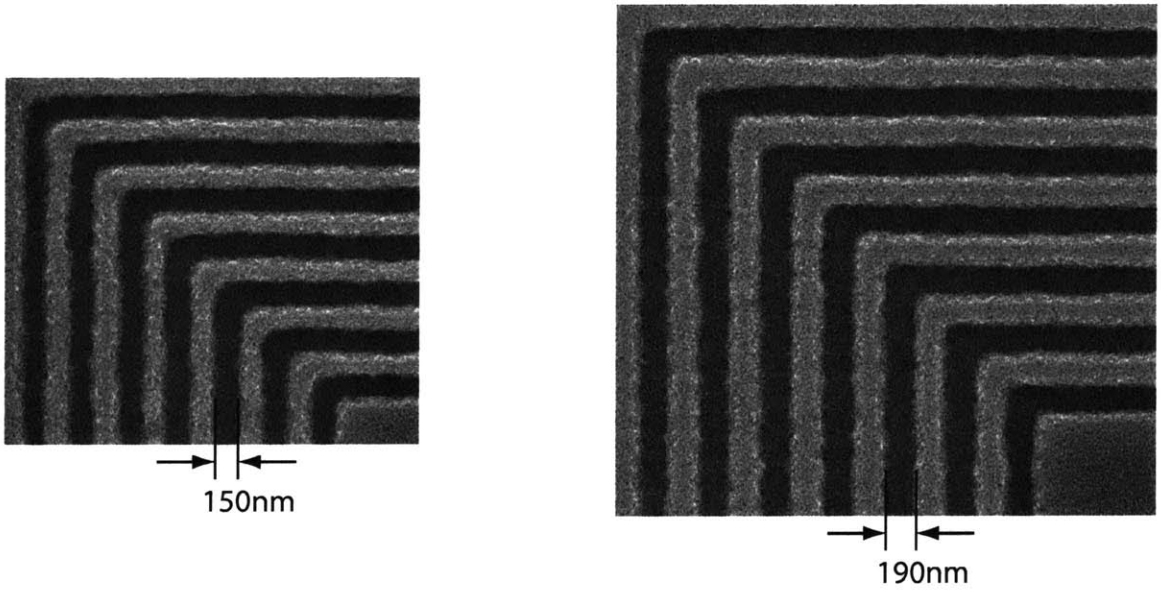

Figure 5-6: Dense nested-L's (150nm and 190nm) patterned with iZPAL.

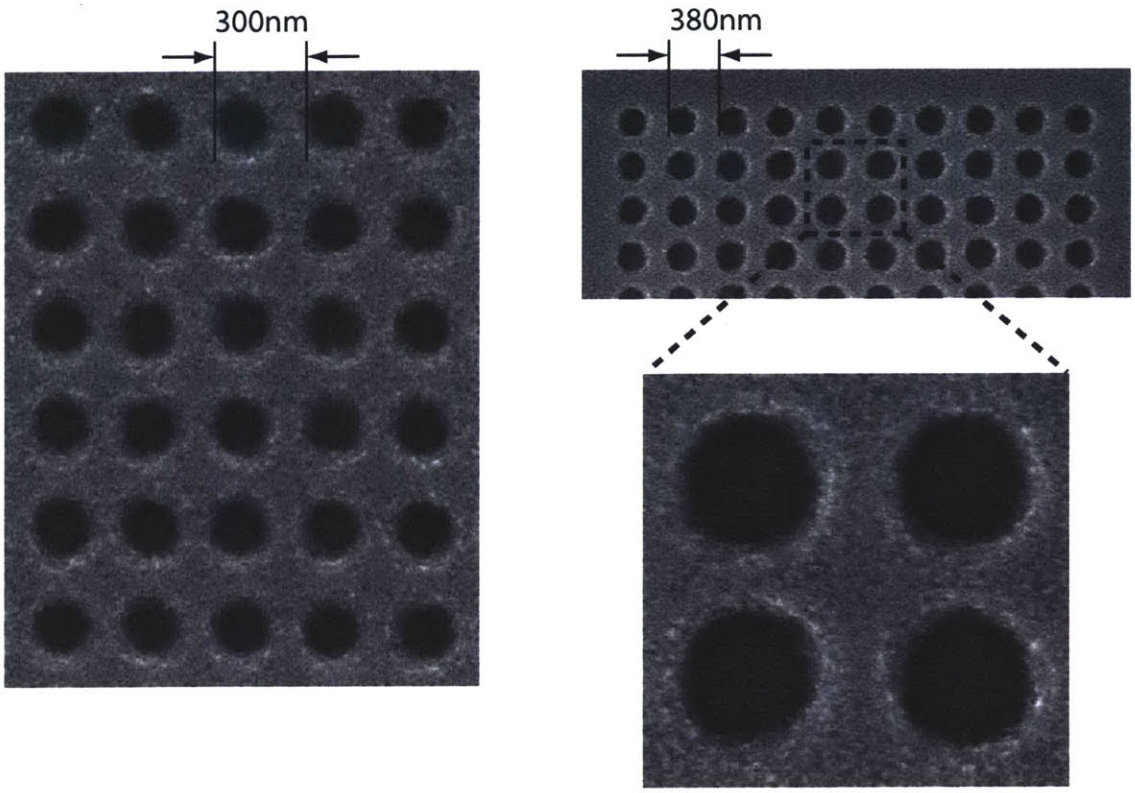

Figure 5-7: Dense array of holes (150nm and 190nm) patterned with iZPAL.

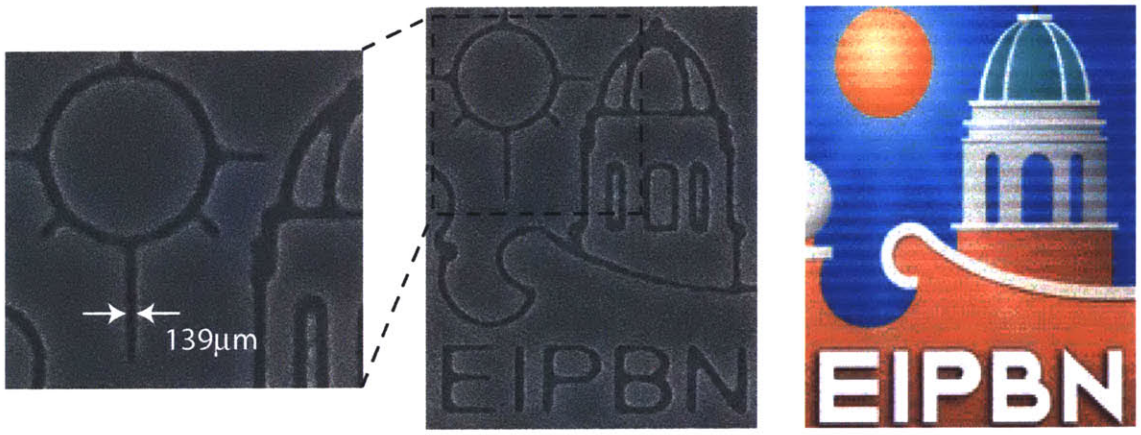

Figure 5-8: Immersion maskless lithographic patterning of the official logo of the Electron, Ion, and Photon Beam Technology and Nanofabrication (EIPBN) conference 2005.

Chapter 6

Conclusion – Future Work

The author hopes that the reader comes away both convinced and encouraged by the immersion maskless lithography technique presented in this thesis. The results demonstrated with this technique help to confirm the immersion scheme's role in improving the performance of lithography systems. While other performance enhancement techniques often times require major system redesign, if not a complete system overhaul, the immersion scheme can be integrated into existent systems with a few relatively straightforward steps. The two-step transformation of ZPAL into iZPAL is a perfect illustration of this. The replacement of air with DI-water as the medium between the zone-plate array and the substrate together with the redesign of the zone plates to focus incident radiation in this new medium completes the transformation and results in improved lithographic performance.

In addition to its relative ease of implementation, the immersion scheme offers the potential for greater, if not unsurpassed, improvements to the performance of lithography systems. In theory, these improvements, which are directly determined by the refractive index of the immersion medium, are limitless. The work presented in this thesis, which makes use of DI-water to improve zone plate focusing (i.e. sharper point-spread function)

and lithographic performance (i.e. increased resolution, exposure latitude, and depth-of-focus), only scratches the surface of the vast realm of possibilities available with such a scheme. Improvements greater than those presented in this thesis can be achieved through the employment of higher refractive index immersion mediums. This is the focus of future work.

6.1 A Potential Solution to an Earlier Problem

Before we delve into the vast realm of prospective immersion setups, a problem encountered with the current setup should first be resolved, as the causes for this problem will probably also plague future setups. The reader may recall from the previous chapter that although the results attained with the immersion scheme demonstrated a marked improvement over those attained with the non-immersion scheme, such improvements, no matter how significant, did not meet theoretical expectations. The causes for this are unknown. However, it was speculated that a possible cause could be the 'pureness' of the DI-water used in the immersion experiments. Recall that the zone plates are designed for a specific $\eta_{DI\text{-}water}$ (refractive index of DI-water). Therefore, any variations to this value will lead to a non-π phase shift between adjacent zones of a zone plate, resulting in non-optimal zone plate focusing.

Up until now, the uncertainty in $\eta_{DI\text{-}water}$ was the only considered explanation for iZPAL's inability to print down to theoretical levels. This is no longer the case, as a second possible cause due to the geometry of the zone plates has come to light [31]. As the immersion medium attempts to fill the circular isolated trenches of a zone plate, the question naturally arises, "what happens to the air there?" There are two logical possibilities. The air either escapes through the immersion medium or remains trapped in the trenches of the zone plate. The latter case, which is depicted in *Figure 6-1*, leads to a multitude of problems, the least of which is the non-π phase shift between adjacent zones. Luckily, the odds of this latter case occurring are rather slim as preliminary calculations have shown that capillary forces are large enough to drive out the air through the DI-water.

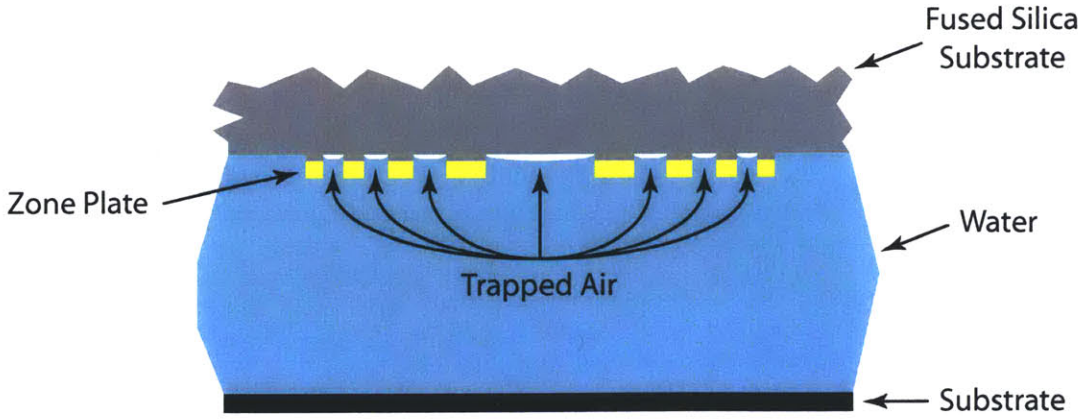

Figure 6-1: An illustration of a potential problem with the current iZPAL experimental setup procedure. As the zone plates are brought into contact with the immersion medium, the air in the zones of the zone plates may become confined as there's no place for it to escape if it cannot do so through the immersion medium.

A simple and straightforward solution has been developed to alleviate the concerns mentioned above. The solution eliminates the need for DI-water filling of the zones as the zones are instead filled with a more reliable medium. Ideally, such a medium possesses a refractive index identical to that of DI-water at the exposing wavelength of radiation. Fortunately, such a medium exists and goes by the name 'Cytop'. Cytop is a spin-on polymer utilized mostly in photonic applications as a cladding layer for waveguides. Its optical properties ($\eta_{Cytop} \approx \eta_{DI\text{-}water} \approx 1.34$ and $k_{Cytop} \approx k_{DI\text{-}water} \approx 0$ at $\lambda = 400nm$), however, also make it an ideal replacement for DI-water in our immersion experiments. *Figure 6-2* illustrates the operation of a zone plate filled with Cytop. The Cytop ensures a π phase shift between adjacent zones of a zone plate. In addition, the Cytop completely fills the zones, as all would-be trapped air is driven out during a high temperature pre-bake step (~ 200 °C). Note that the closeness in the refractive indices of Cytop and DI-water minimizes any light reflections and bending at their interface.

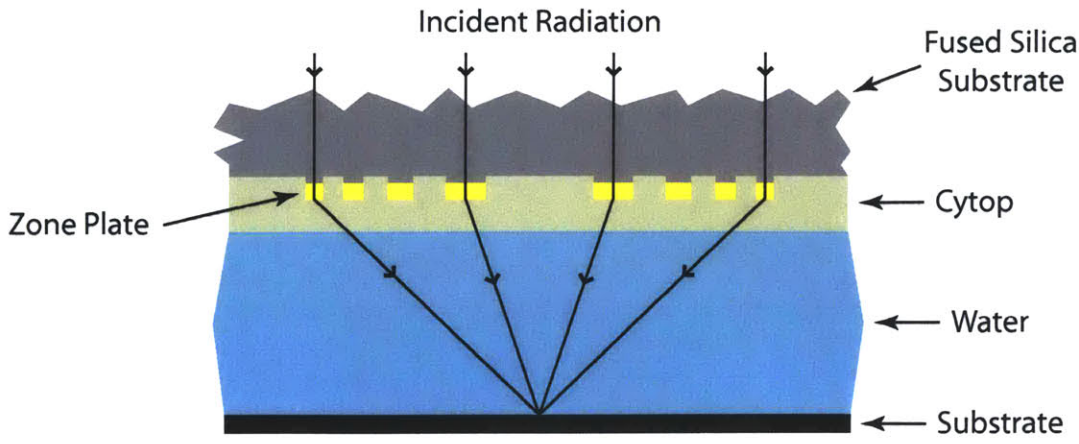

Figure 6-2: The filling of a zone plate with Cytop. Cytop ensures a consistent π phase shift between adjacent zones of a zone plate. It also eliminates the potential for trapped air. Cytop's refractive index at λ = 400nm (the exposing wavelength of radiation) is nearly identical to that of DI-water, thereby minimizing any reflections or bending at their interface.

6.2 Future Immersion Experiments

Now that iZPAL's proof of concept has been demonstrated, the next logical step will be to test the limits of the immersion scheme. In order to do this, high-refractive-index low-absorption mediums are needed. Fortunately, there's a large supply of such mediums on the market today. A good starting point may be to explore mediums already optimized for the field of immersion microscopy. There's no reason why such mediums cannot be exploited for immersion lithography.

Bibliography

[1] M. Lapedus, "$10 million photomask called possible by 2010," *Electronic Engineering Times* **1240**, pp. 22, (2002).

[2] M. Graef, "MEDEA+ efforts on maskless lithography," *Maskless Meeting*, January 2005.

[3] R.E. Howard, H.G. Craighead, L.D. Jackel, P.M. Mankiewich, and M. Feldman, "Electron beam lithography from 20 to 120 kev with a high quality beam," *J. Vac. Sci. Technol. B* **1** (4), pp. 1101-1104, (1983).

[4] Raith150 Operation Manual.

[5] Micronic Laser Systems Sigma7000 Series product line available via URL: <http://www.micronic.se/site_eng/product/semiconductorpr.shtml>

[6] G.E. Moore, "Cramming more components onto integrated circuits," *Electronics Magazine* **38** (8), pp. 114-117, (1965).

[7] International Technology Roadmap for Semiconductors 2004 Update (Lithography) available via URL: <http://www.itrs.net/Common/2004Update/2004_07_Lithography.pdf>

[8] H. Kawata, J.M. Carter, A. Yen, and H.I. Smith, "Optical projection lithography using lenses with numerical apertures greater than unity," *Microelectronic Engineering* **9** (1-4), pp. 31-36, (1989).

[9] J. Mulkens, D. Flagello, B. Streefkerk, and P. Graeupner, "Benefits and limitations of immersion lithography," *Journal of Microlithography, Microfabrication, and Microsystems* **3** (1), pp. 104-114, (2004).

[10] D. Gil and T. Brunner, "First microprocessors printed with immersion lithography," *Microlithography World* **14** (2), pp. 4-7, (2005).

[11] H.I. Smith, "A proposal for maskless, zone-plate-array nanolithography," *J. Vac. Sci. Technol. B* **14** (6), pp. 4318-4322, (1996).

[12] D. Gil, "Maskless nanolithography and imaging with diffractive optical arrays," *Ph.D. Thesis*, Massachusetts Institute of Technology, Cambridge MA, (2003).

[13] R. Menon, "Diffractive optics for maskless lithography and imaging," *Ph.D. Thesis*, Massachusetts Institute of Technology, Cambridge MA, (2003).

[14] R. Menon, A. Patel, E.E. Moon, and H.I. Smith, "An alpha-prototype system for Zone-Plate-Array Lithography," *J. Vac. Sci. Technol. B* **22** (6), pp. 3032-3037, (2004).

[15] Texas Instruments DMD technology available via URL: <http://www.dlp.com/>

[16] Silicon Light Machines GLV™ technology white papers available via URL: <http://www.siliconlight.com/htmlpgs/glvtechframes/glvmainframeset.html>

[17] A.A. Patel, "The development of a prototype Zone-Plate-Array Lithography (ZPAL) system," *S.M. Thesis*, Massachusetts Institute of Technology, Cambridge MA, (2004).

[18] D. Gil, R. Menon, D.J.D. Carter, and H.I. Smith, "Lithographic patterning and confocal imaging with zone plates," *J. Vac. Sci. Technol. B* **18** (6), pp. 2881-2885, (2000).

[19] Lord Rayleigh, *Encyclopaedia Britannica* (9^{th} ed.), Vol. 24, (1998).

[20] J.A. Kong, *Electromagnetic Wave Theory*, EMW Publishing, Cambridge MA, (2000).

[21] A.V. Oppenheim, A.S. Willsky, S.H. Nawab, *Signals & Systems* (2^{nd} ed.), Prentice Hall, Upper Saddle River NJ, (1997).

[22] D. Gil, R. Menon, and H.I. Smith, "Fabrication of high-numerical-aperture phase zone plates with a single lithography exposure and no etching," *J. Vac. Sci. Technol. B* **21** (6), pp. 2956-2960, (2003).

[23] H. Namatsu, T. Yamaguchi, M. Nagase, K. Yamazaki, and K. Kurihara, "Nano-patterning of a hydrogen silsesquioxane resist with reduced linewidth fluctuations," *Microelectronic Engineering* **41-42**, pp. 331-334, (1998).

[24] T.A. Fulton and G.J. Dolan, "New approach to electron beam lithography," *Appl. Phys. Lett.* **42** (8), pp. 752-754, (1983).

[25] G.J. Dolan and T.A. Fulton, "Canyon lithography," *IEEE Electron Dev. Lett.* **4** (6), pp. 178-180, (1983).

[26] T. Barwicz and H.I. Smith, "Evolution of line-edge roughness during fabrication of high-index-contrast microphotonic devices," *J. Vac. Sci. Technol. B* **21** (6), pp. 2892-2896, (2003).

[27] M. Peckerar, R. Bass, and K.W. Rhee, "Sub-0.1 μm electron-beam lithography for nanostructure development," *J. Vac. Sci. Technol. B* **18** (6), pp. 3143-3149, (2000).

[28] J.W. Goodman, *Introduction to Fourier Optics* (2nd ed.), McGraw-Hill, Boston MA, (1996).

[29] R. Menon, D. Gil, and H.I. Smith, "Experimental characterization of focusing by high-numerical-aperture zone plates," submitted to *J. Opt. Soc. Am. A*, (2005).

[30] R. Menon, A. Patel, D. Chao, M. Walsh, and H.I. Smith, "Zone-Plate-Array Lithography (ZPAL): Optical maskless lithography for cost-effective patterning," to be published in *Proc. SPIE*, (2005).

[31] D. Khang and H.H. Lee, "Pressure-assisted capillary force lithography," *Advanced Materials* **16** (2), pp. 176-179, (2004).